Available online at www.sciencedirect.com
ScienceDirect
Geochimica et Cosmochimica Acta 71 (2007) 452–480
Geochimica
www.elsevier.com/locate/gca

Drastic shift in lava geochemistry in the volcanic-front to rear-arc region of the Southern Kamchatkan subduction zone: Evidence for the transition from slab surface dehydration to sediment melting

Svend Duggen [a,*], Maxim Portnyagin [b,c], Joel Baker [d], David Ulfbeck [a], Kaj Hoernle [b], Dieter Garbe-Schönberg [e], Nathalie Grassineau [f]

[a] Geological Institute, University of Copenhagen, Øster Voldgade 10, 1350 Copenhagen K, Denmark
[b] Leibniz Institute for Marine Sciences, IFM-GEOMAR, Division Dynamics of the Ocean Floor, Wischhofstrasse 1-3, 24148 Kiel, Germany
[c] Vernadsky Institute of Geochemistry and Analytical Chemistry (GEOKHI), Russian Academy of Sciences, Kosygin str. 19, Moscow 119991, Russia
[d] School of Earth Sciences, Victoria University of Wellington, P.O. Box 600 Wellington, New Zealand
[e] Institute of Geosciences, University of Kiel, Olshausenstr. 40, 24118 Kiel, Germany
[f] Department of Geology, Royal Holloway College, University of London, Egham, Surrey TW20 OEX, UK

Received 30 May 2006; accepted in revised form 13 September 2006

Abstract

The shift of lava geochemistry between volcanic front to rear-arc volcanoes in active subduction zones is a widespread phenomenon. It is somehow linked to an increase of the slab surface depth of the subducting oceanic lithosphere and increasing thickness of the mantle wedge and new constraints for its causes may improve our understanding of magma generation and element recycling in subduction zones in general. As a case study, this paper focuses on the geochemical composition of lavas from two adjacent volcanic centres from the volcanic front (VF) to rear-arc (RA) transition of the Southern Kamchatkan subduction zone, with the aim to examine whether the shift in lava geochemistry is associated with processes in the mantle wedge or in the subducted oceanic lithosphere or both. The trace element and O–Sr–Nd–Hf–Pb (double-spike)-isotopic composition of the mafic Mutnovsky (VF) and Gorely (RA) lavas in conjunction with geochemical modelling provides constraints for the degree of partial melting in the mantle wedge and the nature of their slab components. Degrees of partial melting are inferred to be significantly higher beneath Mutnovsky (~18%) than Gorely (~10%). The Mutnovsky (VF) slab component is dominated by hydrous fluids, derived from subducted sediments and altered oceanic crust, eventually containing minor but variable amounts of sediment melts. The composition of the Gorely slab component strongly points to a hydrous silicate melt, most likely mainly stemming from subducted sediments, although additional fluid-contribution from the underlying altered oceanic crust (AOC) is likely. Moreover, the Hf–Nd-isotope data combined with geochemical modelling suggest progressive break-down of accessory zircon in the melting metasediments. Therefore, the drastic VF to RA shift in basalt chemistry mainly arises from the transition of the nature of the slab component (from hydrous fluid to melt) in conjunction with decreasing degrees of partial melting within ~15 km across-arc. Finally, systematic variations of key inter-element with high-precision Pb-isotope ratios provide geochemical evidence for a pollution of the Mutnovsky mantle source with Gorely melt components but not vice versa, most likely resulting from trench-ward mantle wedge corner flow. We also present a geodynamic model integrating the location of the Mutnovsky and Gorely volcanic centres and their lava geochemistry with the recently proposed thermal structure of the southern Kamchatkan arc and constraints about phase equilibria in subducted sediments and AOC. Herein, the slab surface hosting the subducted sediments suffers a transition from dehydration to melting above a continuously dehydrating layer of AOC. Wider implications of this study are that an onset of (flush-) sediment melting may ultimately be the main trigger for the VF to RA transition of lava geochemistry in subduction zones.

1. Introduction

The origin of geochemical across-arc zoning of arc lavas attracts the attention of Earth scientists. The phenomenon

* Corresponding author. Present address: Leibniz Institute for Marine Sciences, IFM-GEOMAR, Division Dynamics of the Ocean Floor, Wischhofstrasse 1-3, 24148 Kiel, Germany.
E-mail address: sduggen@ifm-geomar.de (S. Duggen).

0016-7037/$ - see front matter © 2006 Elsevier Inc. All rights reserved.
doi:10.1016/j.gca.2006.09.018

is well expressed in subduction zones with moderate slab angles revealing a major shift in lava geochemistry between the volcanoes at the volcanic front (VF) and those located directly behind in the rear-arc (RA) (e.g., Izu Bonin, Kurile, Kamchatka, Central America) (Ishikawa and Nakamura, 1994; Tatsumi and Eggins, 1995; Walker et al., 1995; Ishikawa and Tera, 1997; Taylor and Nesbitt, 1998; Churikova et al., 2001; Hochstaedter et al., 2001). In terms of major elements the geochemistry changes from high-FeO/MgO and low-K tholeiites in the VF to medium- to low-FeO/MgO, medium- to high-K lavas in the RA. For a given MgO content the RA lavas tend to have higher incompatible trace element concentrations and VF and RA lavas differ significantly as to their inter-element ratios involving both fluid-mobile and relatively immobile elements and isotope ratios (Walker et al., 1995; Ishikawa and Tera, 1997; Taylor and Nesbitt, 1998; Churikova et al., 2001; Hochstaedter et al., 2001). A part of the across-arc geochemical variation may be caused by differences in the degree of partial melting beneath the VF and RA most likely governed by the interplay of water-flux from the subducted slab and decompression of mantle wedge material (Hochstaedter et al., 2001; Portnyagin et al., in press). Further variation may be associated with differences of the source fertility due to mantle wedge corner flow causing the transport of mantle material that has lost a melt component beneath the RA to the VF region for re-melting (Hochstaedter et al., 2001). The role and provenance of slab-derived hydrous fluids and melts as an additional trigger for across-arc geochemical variations is much debated too (Hawkesworth, 1982; Hawkesworth et al., 1993; Pearce and Peate, 1995; Plank and Langmuir, 1998; Pearce et al., 1999; Stern, 2002; Kelemen et al., 2004; George et al., 2005; Plank, 2005). Notably, the release and nature of slab components may be strongly dependent on the thermal structure of the mantle wedge and the subducted oceanic lithosphere.

Recently, geophysical models provided new insights to the thermal structure of active subduction zones. Until then, thermal models predicted that solidus temperatures for sediment and basalt melting were not reached at the top of the subducting plate under normal circumstances. Therefore, slab-surface and ultimately sediment melting became an unpopular melting process since the 1980's to the benefit of fluid-flux melting models and, unfortunately, it even happened that authors for this reason discounted their successful geochemical model involving aqueous silicate slab-melts (see review in Kelemen et al., 2004). However, a fundamentally different picture of the calculated thermal structure of subduction zones arises when the mantle wedge viscosity is not considered constant. Recent thermal models involve non-Newtonian, temperature- and stress-dependent olivine rheology in the mantle wedge and frictional heating of the slab surface before the volcanic front (e.g., for the Central American and southern Kamchatkan arcs) (van Keken, 2003; Manea et al., 2005; Peacock et al., 2005). These models consistently show that mantle material flow is focussed into the tip of the mantle wedge ultimately producing higher temperatures at the slab surface than hitherto thought on the basis of isoviscous models. Intriguingly, the revised thermal structure predicts slab surface temperatures sufficiently high for wet partial melting of subducted sediments and oceanic crust, that therefore appear to be processes more common than hitherto believed (Kelemen et al., 2004). However, if the oceanic crust is covered by a layer of marine sediments, partial melting may be restricted to the sediment layer whereas the basaltic oceanic crust only dehydrates (Peacock et al., 2005). It is worth noting that the differences in predicted slab surface temperatures arising from the two groups of thermal models seem to be particularly relevant for the inferred thermal conditions of the slab surface beneath the volcanic front to rear-arc region (van Keken, 2003; Manea et al., 2005; Peacock et al., 2005).

In order to examine the role of crustal and mantle processes, we performed an extensive trace element and isotope (O–Sr–Nd–Hf–Pb double-spike) study focussing on the Mutnovsky (VF) and Gorely (RA) volcanoes in southern Kamchatka. This arc segment is ideal for such a study because: (1) it has a moderate slab angle of ~55° (Gorbatov et al., 1997) not too shallow to inhibit arc magmatism and not too steep to produce an unfavourable overlap of possible zones of slab-derived fluid and melt mobilisation, (2) it is a relatively simple subduction zone segment aside the complicating influence of a slab edge and subducting seamount chain as is the case further north in the Kamchatkan subduction zone (Dorendorf et al., 2000; Churikova et al., 2001; Yogodzinski et al., 2001; Portnyagin et al., 2005), (3) a model for the thermal structure of its mantle wedge was published recently predicting the possibility of sediment melting at the slab surface (Manea et al., 2005) and (4) the Mutnovsky and Gorely stratovolcanoes are located above the predicted region of slab surface melting just ~15 km apart along an across-arc profile. This paper provides new insights to the magma genesis and element recycling in the Kamchatkan arc in particular and subduction zones in general confirming the predictions of recent thermal models.

2. Geological background

The Kamchatkan peninsula is one of the most active volcanic realms on Earth. Two volcanic zones can be distinguished (Fig. 1): The Sredinny Range (SR) and the Eastern volcanic belt (EVB) located south of the Bering-Alpha Fault Zone. The EVB can be subdivided into a northern, central and southern segment. The former is hosting the Central Kamchatkan Depression (CKD) and the other are separated by the Petropavlovsk Fault zone. The southern part of the EVB continues into the northern Kurile arc situated due south of the Kamchatkan peninsula. Most of the active Kamchatkan volcanoes are found in the arcuate EVB that is formed largely parallel to the Kurile-Kamchatkan trench where the Pacific plate is sub-

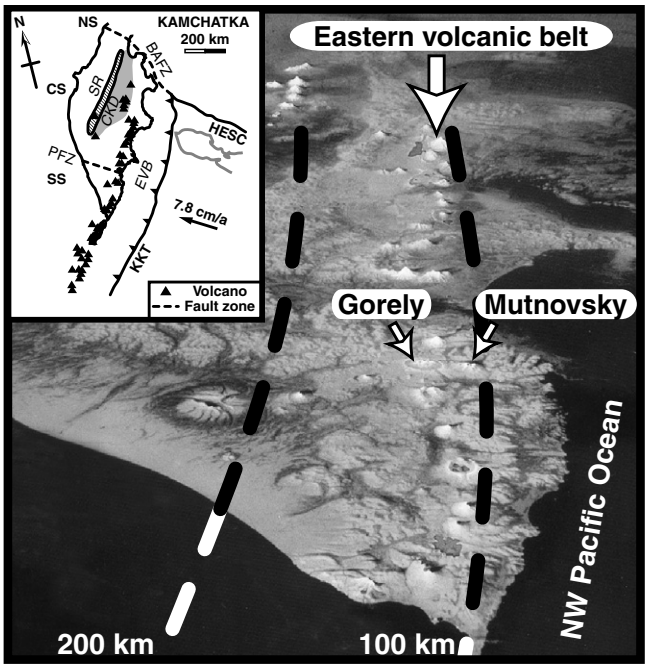

Fig. 1. Space image of the Kamchatkan peninsula (NASA) showing the Mutnovsky and Gorely volcanic centres in the Eastern volcanic belt. These stratovolcanoes constitute the volcanic front to rear-arc transition of an ~80 km long across-arc volcanic chain in southern Kamchatka. Stippled lines indicate slab surface depths. The inset gives an overview of the geodynamic situation in Kamchatka and the northwesternmost Pacific Ocean (modified from Ishikawa et al. (2001)). Abbreviations are: NS, Northern Segment; CS, Central Segment; SS, Southern Segment; BAFZ, Bering-Aleutian Fault Zone; SR, Sredinny Ridge; CKD, Central Kamchatkan Depression; PFZ, Petropavlovsk Fault Zone; KKT, Kurile-Kamchatka Trench; HESC, Hawaii-Emperor Seamount Chain.

ducted with ~7.8 cm/y (Gorbatov et al., 1997, 1999). Along the volcanic front of southern Kamchatka the volcanic centres are situated ~90–110 km above the Wadati-Benioff Zone, whereas the rear-arc volcanoes are located above slab surface depths ranging from ~100–220 km (Fig. 1).

Several pairs of volcanoes exist in the Kamchatkan arc revealing a geochemical shift between the VF and RA region. From north to south, examples are Klyuchevskoy–Ushkovsky, Zhupanovsky–Dzenzursky, Avachinsky–Koryaksky, Mutnovsky–Gorely and Kambalny–Kosheleva (Fedotov and Masurenkov, 1991; Hochstaedter et al., 1996) suggesting that the shift is related to systematic across-arc changes in the chemical and physical conditions of the Kamchatkan subduction zone. The Holocene Mutnovsky and Gorely volcanic centres are located in the southern segment and are part of an ~80 km long east–west oriented across-arc volcanic chain (Fig. 1). The Mutnovsky stratovolcano is situated ~100 km above the surface of the subducting slab, whereas the Gorely volcano, hosting a caldera, is displaced ~15 km westward and therefore located ca. 120 km above the slab surface (Selyangin, 1993; Selyangin and Ponomareva, 1999). In contrast to Central Kamchatka, comprehensive geochemical data sets with major and trace element and radiogenic and stable isotope data barely exist for southern Kamchatkan arc lavas. Until this study the geochemically most well studied volcanic centre in this area is Ksudach volcano (Bailey et al., 1987; Bindeman et al., 2004), whereas for Mutnovsky and Gorely only few selected samples have been analysed that include both major and trace element concentrations and isotope ratios (Kepezhinskas et al., 1997; Turner et al., 1998; Pineau et al., 1999; Bindeman et al., 2004).

3. Results

Major and trace element whole rock data were determined by X-ray fluorescence analysis (XRF), inductively coupled-plasma mass spectrometry (ICP-MS) and isotope dilution (ID) mass spectrometry using a multi collector (MC)-ICP-MS (Tables 1–3). Oxygen isotope ratios of mineral separates were determined by means of CO_2-laser flourination mass spectrometry (Table 4). Radiogenic isotope whole rock data were analysed by TIMS (Sr) and MC-ICP-MS (Nd, Hf and Pb double-spike) (Table 4). The analytical methods and procedures are comprehensively described in Appendix A.

3.1. Major and trace element data

The lavas from the Mutnovsky and Gorely volcanic centres have completely different major and trace element compositions. They, respectively, range from 49.1–60.1 and 50.3–76.8 wt% SiO_2 and from 2.1–6.9 and 0.3–9.2 wt% MgO. Based on their major element contents, the mafic Mutnovsky lavas are mostly high-Fe tholeiites whereas most Gorely samples are medium-Fe, medium- to high-K basalts to trachyandesites (Fig. 2a and b). Positive correlations of MgO with CaO, Sc, Cr and Ni (Fig. 2) point to the significant role of combined olivine and clinopyroxene fractional crystallisation yet there is no evidence for phenocryst accumulation. Kinks in diagrams with MgO versus SiO_2, TiO_2, FeO, P_2O_5, V, Zn, Ga, Y and Zr illustrate the onset of magnetite, apatite and zircon fractional crystallisation below 2–4 wt% MgO. Lavas from Mutnovsky (except one more evolved sample) do not have significant Eu-anomalies [$Eu/Eu^* = (Eu_{Nch})/(Sm_{Nch} * Gd_{Nch})^{1/2}$, Nch—normalised to chondrite] but those from Gorely have Eu/Eu^* ranging from 0.96 to 0.78 correlating positively with CaO and Sr/Nd due to substantial fractional crystallisation of plagioclase even in basaltic samples (except the most mafic lava N69) (Fig. 3j). For a given MgO content the mafic Mutnovsky samples (>4% MgO) generally have higher Al_2O_3, FeO, MnO, CaO, Co and V but lower SiO_2, Na_2O, K_2O, P_2O_5, Cr, (±Ni) and both fluid-mobile and fluid-immobile, incompatible element contents (e.g., Cs, Tl, Rb, Ba, Th, U, Nb, Pb, Sn, Zr, Hf, Y and REE) than Gorely lavas (Figs. 2–4).

In multi-element diagrams, Mutnovsky (M) and Gorely (G) arc lavas have spiked patterns with incompatible ele-

Table 1
Major (wt%) and trace element (ppm) XRF data of Mutnovsky and Gorely lavas

Sample no.	N72	N75	N73	N71	N74	N79	N94	N78	N98	N77	N95	N69
Location	Mutnovsky	Mutnovsky	Mutnovsky	Mutnovsky	Mutnovsky	Mutnovsky	Mutnovsky	Mutnovsky	Mutnovsky	Mutnovsky	Mutnovsky	Gorely/ Dvugorbaya
Latitude N	52.473	52.479	52.473	52.473	52.473	52.502	52.468	52.479	52.476	52.479	52.474	52.531
Longitude E	158.137	158.132	158.137	158.137	158.137	158.128	158.164	158.135	158.158	158.131	158.161	158.134
Age	Q_3	Q_3	Q_3	Q_3	Q_3	Q_3	Q_3	Q_3	Q_3	Q_3	Q_3	Q_3
Rock type	Basalt	Basalt	Basalt	Basalt	Basalt	Bas. andesite	Basalt	Bas. andesite	Bas. andesite	Andesite	Andesite	Basalt
SiO_2	49.1	50.3	49.6	50.1	50.2	52.2	50.8	52.5	53.5	58.5	60.1	50.3
TiO_2	0.88	0.88	0.99	0.97	1.00	1.24	1.05	0.98	1.23	0.96	0.88	1.05
Al_2O_3	18.0	18.4	18.4	18.8	18.4	17.0	18.0	18.6	16.9	16.0	17.2	15.9
Fe_2O_{3t}	10.2	9.95	10.9	10.5	11.1	10.6	11.3	9.65	11.4	9.42	6.98	10.2
MnO	0.17	0.17	0.18	0.18	0.18	0.18	0.21	0.18	0.21	0.23	0.12	0.17
MgO	6.88	5.93	5.60	5.31	5.30	4.86	4.71	4.11	3.80	2.60	2.12	9.22
CaO	11.1	10.0	10.4	10.7	10.5	9.12	9.87	9.34	8.05	5.98	6.58	9.07
Na_2O	2.40	2.63	2.70	2.77	2.69	3.46	2.82	3.00	3.59	4.48	3.69	2.90
K_2O	0.22	0.44	0.33	0.33	0.38	0.91	0.26	0.62	0.44	0.93	1.82	0.93
P_2O_5	0.15	0.18	0.13	0.14	0.17	0.34	0.17	0.21	0.21	0.21	0.21	0.29
H_2O	0.80	0.83	0.49	0.21	0.44	0.21	1.05	0.98	0.47	0.49	0.28	0.18
CO_2	0.03	0.08	0.03	0.01	0.03	0.01	0.03	0.21	0.05	0.04	0.04	0.02
Sum	99.9	99.9	99.7	100.1	100.4	100.1	100.3	100.4	99.8	99.8	100.1	100.2
Co	46	37	38	42	38	30	40	34	35	22	15	44
Cr	123	86	67	59	63	69	50	53	19	<18	<18	366
Ni	68	39	20	34	10	10	9	20	<2	<2	4	142
V	296	327	340	332	329	300	343	282	321	189	151	249
Zn	76	76	89	88	90	85	99	81	107	113	70	82
Ce	21	19	22	<10	20	20	12	14	17	25	20	41
La	<14	<14	<14	<14	<14	<14	<14	<14	<14	<14	<14	<14
Nb	2	4	3	3	2	6	3	3	5	5	7	7
Ga	16	20	18	19	16	17	21	18	21	22	19	15
Pb	6	8	9	17	9	6	5	8	6	14	9	11
Pr	<4	<4	<4	<4	<4	<4	<4	<4	<4	<4	<4	<4
Rb	<4	7	5	4	5	13	<4	11	8	16	35	16
Ba	112	146	120	154	149	309	158	261	168	313	470	313
Sr	419	408	402	417	412	464	420	436	409	376	357	437
Th	<4	<4	<4	6	<4	<4	<4	<4	<4	<4	<4	5
Y	21	20	22	23	24	28	25	24	28	41	35	24
Zr	52	61	55	54	58	111	62	82	75	113	162	96

(*continued on next page*)

Table 1 (*continued*)

	N87	N89	N88	N65-A	N62	N65-B	N57	N56	N63	N67	N66	N84
Location	Gorely	Gorely	Gorely	Gorely	Gorely	Gorely	Gorely	Gorely	Gorely	Gorely	Gorely	Gorely
Latitude N	52.559	52.591	52.580	52.544	52.548	52.544	52.559	52.559	52.548	52.545	52.545	52.589
Longitude E	158.043	157.996	157.992	158.016	158.000	158.016	158.017	158.017	158.000	158.032	158.022	158.000
	Q_{3-4}	Q_4	8–11 Ky	Q_4(?)	8–11 Ky	Q_4(?)	Q_4(?)	Q_4	8–11 Ky	~250 BP	Q_4(?)	3000 BP
Rock type	Bas. andesite	Bas. andesite	Bas. andesite	Bas. andesite	Bas. andesite	Bas. andesite	Bas. andesite	Bas. andesite	Bas. andesite	Bas. andesite	Bas. andesite	Bas. andesite
SiO_2	53.6	53.2	53.0	53.8	53.9	54.8	55.3	54.9	54.8	54.3	54.2	55.3
TiO_2	1.17	1.10	1.06	1.21	1.03	1.25	1.23	1.24	1.04	1.24	1.22	1.22
$A1_2O_3$	16.4	17.1	17.4	16.8	17.3	16.6	16.5	16.6	17.1	16.4	16.5	16.4
Fe_2O_{3t}	9.83	9.49	9.58	9.77	8.96	9.54	9.49	9.47	8.94	9.47	9.62	9.17
MnO	0.16	0.17	0.17	0.15	0.16	0.16	0.16	0.16	0.16	0.16	0.15	0.16
MgO	5.43	5.21	5.13	4.75	4.62	4.52	4.51	4.50	4.47	4.46	4.44	4.37
CaO	7.71	8.19	8.63	7.98	8.27	7.46	7.60	7.50	7.86	7.37	7.37	7.21
Na_2O	3.23	3.32	3.22	3.13	3.28	3.39	3.36	3.45	3.34	3.45	3.41	3.46
K_2O	1.64	1.35	1.16	1.67	1.39	1.94	1.84	1.93	1.51	1.93	1.89	2.01
P_2O_5	0.41	0.37	0.33	0.42	0.29	0.44	0.42	0.45	0.30	0.46	0.45	0.44
H_2O	0.37	0.59	0.42	0.68	0.52	0.14	0.25	0.24	0.45	0.25	0.56	0.24
CO_2	0.03	0.04	0.03	0.04	0.03	0.02	0.05	0.04	0.03	0.02	0.04	0.01
Sum	100.0	100.1	100.1	100.4	99.8	100.3	100.7	100.5	100.1	99.5	99.8	100.0
Co	31	32	29	28	27	26	25	26	25	28	26	24
Cr	166	90	97	95	80	95	81	101	85	100	95	109
Ni	66	31	28	26	8	27	21	29	19	28	42	29
V	237	240	259	246	242	224	235	226	235	225	224	217
Zn	85	82	86	89	78	84	87	82	73	82	88	80
Ce	29	26	11	37	21	41	50	31	35	59	26	58
La	<14	<14	<14	<14	16	<14	<14	<14	<14	<14	<14	<14
Nb	8	7	6	8	3	8	8	8	6	8	8	7
Ga	14	17	20	15	16	19	16	18	19	18	20	15
Pb	10	10	8	8	11	13	9	10	7	6	11	7
Pr	<4	<4	<4	<4	<4	<4	<4	<4	<4	<4	<4	<4
Rb	29	24	19	33	26	39	35	35	29	37	36	39
Ba	470	457	397	510	405	526	524	536	428	532	520	548
Sr	422	499	470	450	446	429	408	437	432	432	425	416
Th	<4	<4	<4	<4	<4	<4	<4	4	<4	<4	<4	<4
Y	35	29	29	32	27	36	34	38	27	37	35	36
Zr	179	147	134	180	131	215	200	214	145	211	203	219

Location	N55 Gorely	N90 Gorely	N80 Gorely	N92 Gorely	N64 Gorely	N60 Gorely	N59 Gorely	N61 Gorely	N68 Gorely	N86 Gorely	N82 Gorely	N58 Gorely	N70 Gorely / Skalistaya
Latitude N	52.583	52.523	52.571	52.517	52.547	52.552	52.560	52.549	52.545	52.549	52.571	52.576	
Longitude E	158.016	157.958	158.010	157.951	158.006	157.988	157.972	157.998	158.032	158.064	158.002	157.971	
	8–11 Ky	~250 BP	Q_3 (?)	~250 BP	~250 BP	~250 BP	~250 BP	~250 BP	Q_3	~250 BP	Q_3	Q_2	63-68 Ky
Rock type	Bas. andesite	Bas. andesite	Bas. andesite	Trachyan-desite	Trachyan-desite	Trachyan-desite	Trachyan-desite	Trachyan-desite	Andesite	Trachyan-desite	Trachyte	Rhyolite	Rhyolite
SiO_2	55.9	56.8	56.9	57.3	57.3	57.2	57.8	57.2	58.1	57.6	60.4	68.9	76.8
TiO_2	1.24	1.37	1.24	1.39	1.38	1.37	1.40	1.37	1.39	1.39	1.29	0.69	0.19
Al_2O_3	16.3	15.9	16.2	15.9	15.9	16.0	16.1	16.2	16.4	15.9	15.3	15.0	12.2
Fe_2O_{3t}	9.27	9.25	8.82	9.18	9.00	8.89	9.02	9.06	8.79	9.00	7.74	2.75	1.24
MnO	0.16	0.16	0.16	0.16	0.15	0.16	0.16	0.15	0.14	0.15	0.16	0.12	0.04
MgO	4.29	3.15	3.09	2.94	2.90	2.89	2.87	2.85	2.78	2.75	2.17	0.79	0.27
CaO	7.00	6.41	6.35	6.19	6.19	6.24	6.18	6.26	6.11	6.02	4.71	1.83	1.03
Na_2O	3.52	3.56	3.99	3.73	3.69	3.75	3.82	3.73	3.36	3.75	4.54	5.44	3.96
K_2O	2.12	2.48	1.88	2.61	2.59	2.58	2.65	2.58	2.14	2.71	2.51	3.30	3.36
P_2O_5	0.46	0.52	0.42	0.54	0.53	0.54	0.54	0.53	0.48	0.56	0.51	0.13	0.03
H_2O	0.38	0.24	0.70	0.18	0.28	0.27	0.28	0.24	0.26	0.24	0.28	0.35	0.38
CO_2	0.05	0.03	0.01	0.01	0.03	0.04	0.03	0.02	0.03	0.01	0.01	0.03	0.04
Sum	100.7	99.9	99.8	100.1	99.9	99.9	100.9	100.2	100.0	100.1	99.6	99.3	99.5
Co	24	22	20	19	18	17	19	20	22	16	11	4	5
Cr	109	31	<18	<18	21	27	31	27	49	<18	<18	<18	<18
Ni	39	10	5	5	<2	3	3	19	11	6	<2	<2	<2
V	208	214	254	217	201	205	210	212	231	204	161	41	16
Zn	86	85	83	87	88	88	89	88	83	91	86	66	29
Ce	56	50	28	48	56	42	60	64	51	57	47	73	20
La	<14	<14	16	21	18	<14	<14	<14	<14	17	<14	<14	<14
Nb	8	9	8	10	9	11	13	11	8	11	9	6	<2
Ga	19	17	17	14	16	21	16	15	19	17	17	15	10
Pb	8	14	11	17	9	17	12	13	13	12	14	11	11
Pr	<4	<4	<4	<4	7	<4	<4	<4	<4	6	5	13	<4
Rb	41	48	35	53	53	53	53	51	41	55	43	60	66
Ba	583	681	571	683	694	688	671	688	621	694	748	879	821
Sr	404	373	424	364	366	368	362	372	411	361	354	200	87
Th	<4	6	<4	5	4	<4	5	<4	<4	<4	<4	<4	8
Y	39	44	35	48	45	46	48	47	37	47	48	51	16
Zr	229	280	199	293	292	293	295	292	246	306	266	340	121

Abbreviations: Q, Quaternary; Q_1, Early Pleistocene; Q_2, Middle Pleistocene; Q_3, Late Pleistocene; Q_4, Holocene.

Table 2
ICP-MS trace element data (ppm) of selected Mutnovsky (M) and Gorely (G) lavas and altered oceanic crust samples (K-AOC)

Location	M	M	M	M	M	M	M	M	G	G	G	G	G	G	G	Kronotsky Peninsula	Kamchatsky Peninsula	Kamchatsky Peninsula
Sample no.	N72	N75	N71	N79	N94	N78	N98	N77	N69	N87	N89	N88	N84	N86	N58	881	6539-4	D210-1
Rock type	B	B	B	BA	B	BA	BA	A	B	BA	BA	BA	BA	TA	R	AM	AM	AM
Li	5.57	6.16	6.16	7.55	4.76	5.49	7.05	13.2	6.59	9.92	9.65	9.35	11.6	16.4	22.5	6.37	10.2	20.3
Sc	38.4	33.1	39.0	34.6	34.1	29.1	39.7	27.7	32.5	27.3	27.4	29.6	25.0	23.9	12.0	51.1	38.9	45.7
V	391	312	438	288	316	269	300	169	336	228	239	252	210	205	28.0	478	240	254
Cr	120	69.7	49.7	49.1	28.8	31.6	2.06	0.80	359	152	80.7	88.0	93.8	13.3	1.16	212	393	535
Co	36.0	28.8	30.9	25.4	27.4	24.0	23.0	14.5	42.7	30.3	26.5	26.8	22.8	17.9	1.61	47.6	31.4	61.8
Ni	51.5	29.8	24.7	16.7	14.9	21.0	3.81	6.53	156	69.7	42.2	36.0	42.0	11.3	2.36	87.6	99.9	216
Cu	131	125	105	78.9	128	107	105	71.5	90.3	77.0	83.3	88.4	86.3	109	4.36	61.4	14.7	86.3
Zn	77.6	75.1	88.5	81.9	90.9	76.6	105	106	81.0	82.7	80.7	81.8	80.3	89.2	64.7	127	47.0	92.3
Ga	18.2	16.8	20.4	17.3	18.2	17.6	19.4	19.0	17.1	16.6	17.3	17.5	17.0	18.0	16.8	21.4	13.8	17.0
Rb	2.87	4.65	3.76	12.0	3.48	7.97	5.17	12.4	14.4	28.8	21.6	17.3	36.9	53.2	55.2	0.41	3.64	7.32
Sr	430	404	433	459	408	429	406	367	454	427	508	476	416	365	201	117	170	171
Y	17.3	18.3	20.0	25.6	21.4	21.6	26.7	37.5	22.4	32.0	26.2	25.5	33.9	43.8	44.7	57.0	24.6	25.6
Zr	44.2	51.3	43.8	103	50.6	76.1	59.0	105	95.3	178	148	130	216	301	338	177	60.4	63.5
Nb	0.99	1.18	0.86	2.89	0.97	1.70	1.13	1.70	2.89	4.96	4.50	3.70	5.94	8.25	9.71	4.11	1.19	0.65
Mo	0.31		0.43						0.65							0.47	0.10	0.23
Sn	0.60	1.05	0.70	0.95	1.23	0.98	0.85	1.36	0.89	1.44	1.15	1.34	1.60	2.79	2.69	1.55	0.41	0.53
Sb	0.15	0.14	0.15	0.09	0.18	0.21	0.28	0.44	0.06	0.19	0.12	0.11	0.27	0.41	0.40			
Cs	0.25	0.16	0.34	0.39	0.29	0.40	0.29	1.01	0.46	0.60	0.83	0.69	1.60	2.36	2.11	0.01	0.08	0.35
Ba	110	196	126	343	169	278	180	316	284	476	498	412	564	732	911	6.11	66.6	17.6
La	3.87	4.72	3.62	10.0	4.28	6.78	4.79	7.35	9.51	15.8	14.5	12.5	18.6	24.9	26.3	5.27	1.85	1.54
Ce	10.5	12.4	10.2	25.2	12.0	17.1	13.7	21.2	23.7	38.4	35.1	30.3	44.9	59.7	62.1	17.5	6.28	5.59
Pr	1.69	1.99	1.72	3.80	2.04	2.62	2.39	3.66	3.44	5.56	5.02	4.35	6.35	8.40	8.44	3.15	1.13	1.13
Nd	8.54	10.1	8.97	18.2	10.8	12.9	12.8	19.2	15.8	25.3	22.7	20.0	28.7	37.1	36.1	16.8	6.22	6.46
Sm	2.51	2.89	2.72	4.68	3.25	3.48	3.88	5.63	3.99	6.11	5.39	4.83	6.76	8.67	8.08	5.70	2.26	2.33
Eu	0.87	1.01	0.96	1.52	1.15	1.15	1.37	1.71	1.22	1.63	1.58	1.45	1.72	2.01	1.91	1.96	0.80	0.97
Gd	2.72	3.30	3.05	5.01	3.76	3.86	4.54	6.31	3.93	6.29	5.44	4.98	6.87	8.69	7.86	7.29	2.97	3.11
Tb	0.47	0.56	0.53	0.82	0.64	0.65	0.78	1.09	0.64	1.00	0.86	0.79	1.09	1.38	1.29	1.34	0.56	0.58
Dy	2.98	3.57	3.41	5.06	4.17	4.08	5.09	6.99	3.87	6.11	5.27	4.89	6.62	8.36	8.09	8.87	3.76	3.87
Ho	0.62	0.75	0.71	1.05	0.88	0.85	1.07	1.48	0.79	1.26	1.08	1.00	1.37	1.71	1.70	1.87	0.79	0.82
Er	1.74	2.08	2.01	2.89	2.47	2.39	3.03	4.21	2.20	3.48	2.98	2.78	3.80	4.81	4.92	5.30	2.24	2.32
Tm	0.25	0.31	0.29	0.43	0.37	0.36	0.45	0.65	0.32	0.52	0.45	0.42	0.57	0.72	0.77	0.80	0.33	0.34
Yb	1.68	2.14	1.96	2.88	2.51	2.43	3.08	4.40	2.12	3.53	3.06	2.81	3.87	4.87	5.41	5.35	2.20	2.30
Lu	0.25	0.32	0.29	0.44	0.38	0.37	0.47	0.67	0.31	0.53	0.46	0.43	0.59	0.74	0.83	0.80	0.32	0.34
Hf	1.30	1.55	1.36	2.69	1.61	2.05	1.89	3.16	2.46	4.39	3.77	3.19	5.43	7.43	8.10	4.26	1.49	1.51
Ta	0.05	0.08	0.05	0.18	0.06	0.11	0.07	0.11	0.16	0.31	0.29	0.24	0.38	0.52	0.63	0.24	0.07	0.04
W	0.06		0.08						0.10									
Tl	0.05	0.02	0.04	0.05	0.02	0.09	0.06	0.07	0.04	0.11	0.12	0.10	0.17	0.22	0.31	0.01	0.02	0.05
Pb	2.85	3.84	2.99	4.54	3.78	5.42	4.08	6.41	3.85	6.20	6.49	6.19	9.03	12.7	14.2	0.59	0.01	0.13
Th	0.21	0.26	0.22	0.89	0.24	0.69	0.28	0.77	1.04	2.27	1.65	1.34	2.97	4.37	4.04	0.26	0.06	0.04
U	0.12	0.13	0.12	0.38	0.14	0.31	0.15	0.37	0.40	0.93	0.67	0.56	1.21	1.79	1.65	0.11	0.03	0.09

Abbreviations: B, basalt; BA, basaltic andesite; A, andesite; TA, trachyandesite; R, rhyolite; AM, altered MORB.

Table 3
MC-ICP-MS isotope dilution trace element data (ppm) of selected Mutnovsky and Gorely lavas

Sample no.	N72	N75	N73	N71	N74	N79	N94	N78	N98	N77	N69	
Location	Mutnovsky	Mutnovsky	Mutnovsky	Mutnovsky	Mutnovsky	Mutnovsky	Mutnovsky	Mutnovsky	Mutnovsky	Mutnovsky	Gorely	
Rock type	Basalt	Basalt	Basalt	Basalt	Basalt	Bas. andesite	Basalt	Bas. andesite	Bas. andesite	Andesite	Basalt	
Rb	2.00	4.40	3.86	3.54	4.03	11.2	3.18	7.43	4.60	11.7	12.6	
Ba	96.5	192	165	136	150	321	157	262	161	304	304	
Th	0.122	0.228	0.182	0.153	0.199	0.573	0.198	0.643	0.204	0.644	1.04	
U	0.127	0.151	0.153	0.129	0.146	0.349	0.155	0.413	0.170	0.382	0.401	
La	4.65	5.53	3.68	3.70	4.64	10.9	4.13	7.92	4.63	7.88	12.3	
Ce	11.1	12.9	10.4	10.3	12.0	25.2	11.4	18.0	12.9	22.0	26.4	
Pb	2.33	3.01	2.69	2.43	2.71	3.57	2.96	5.04	3.01	5.99	3.30	
Nd	8.63	9.71	9.00	8.89	9.91	17.0	9.83	12.6	11.4	18.9	16.2	
Sr		399		407	417	452	394	426	380	366	410	
Sm	2.48	2.74	2.73	2.67	2.94	4.35	2.92	3.38	3.44	5.51	3.97	
Hf	1.37	1.55	1.37	1.42	1.55	2.68	1.62	2.14	1.92	3.30	2.44	
Eu	0.880	0.960	0.991	0.967	1.03	1.54	1.04		1.22		1.24	
Gd	2.82	3.09	3.17	3.05	3.38	4.53	3.48		4.13		3.94	
Dy	3.00	3.28	3.49	3.39	3.66	4.84	3.71	3.97	4.40		3.96	
Er	1.85	2.03	2.18		2.34	2.91	2.31	2.45	2.76	4.01	2.36	
Yb	1.70	1.89	2.01	1.97	2.16	2.69	2.17	2.32	2.60	3.90	2.18	
Lu	0.249	0.277	0.295	0.292	0.321	0.392	0.317	0.347	0.387	0.584	0.317	

Sample no.	N87	N89	N88	N67	N84	N55	N90	N80	N60	N86	N82	N58
Location	Gorely	Gorely	Gorely	Gorely	Gorely	Gorely	Gorely	Gorely	Gorely	Gorely	Gorely	Gorely
Rock type	Bas. andesite	Bas. andesite	Bas. andesite	Bas. andesite	Bas. andesite	Bas. andesite	Bas. andesite	Bas. andesite	Trachyandesite	Trachyandesite	Trachyte	Rhyolite
Rb	24.9	20.1	16.5	33.5	34.4	36.4	45.3	29.5	43.9	49.3	40.2	52.3
Ba	436	469	402	551	525	569	658	566	691	689	725	913
Th	1.58	1.30	1.02	2.31	2.35	2.36		2.08	2.57	3.34	2.83	3.46
U	0.887	0.646	0.544	1.13	1.09	1.24		0.963	1.41	1.53	1.31	1.60
La	17.2	17.0	14.1	18.3	18.3	19.0	24.9	16.9	23.3	24.2	22.6	26.7
Ce	39.7	35.7	32.2	44.0	44.1	45.8	56.2	41.2	56.3	57.9	53.5	62.9
Pb	5.57	5.50	5.25	7.94	7.82	8.50		7.61	9.95	10.7	10.0	13.4
Nd	24.6	21.2	20.0	27.0	26.8	27.7	33.4	25.0	33.7	34.5	32.0	35.1
Sr	388			430	407	397		418	339	357		198
Sm	5.98	4.96	4.80	6.34	6.28	6.48	7.76	5.87	7.81	8.00	7.43	7.81
Hf	4.50	3.63	3.30	5.09	5.31	5.65	6.84	4.82	7.13	7.39	6.23	8.47
Eu	1.57	1.46	1.44	1.62	1.60	1.62	1.85	1.66	1.84		1.96	1.85
Gd	5.73	4.75	4.60	5.95	5.99	6.51	7.14	5.55	7.24		6.82	6.68
Dy	5.79	4.72	4.74	6.08	6.05	6.32	7.21	5.61	7.38		7.20	7.60
Er	3.50	2.83	2.89	3.65	3.65	3.81	4.37	3.42	4.45	4.60	4.47	4.89
Yb	3.27	2.65	2.69	3.44	3.44	3.61	4.11	3.26	4.21	4.35	4.22	5.00
Lu	0.459	0.389	0.389	0.504	0.506	0.532	0.585	0.468	0.606	0.632		0.742

Table 4
O–Sr–Nd–Hf–Pb (double spike) isotope data of Mutnovsky and Gorely lavas and Sr–Nd–Pb (conventional) Kamchatka]! Pacific altered oceanic crust (K-AOC)

Sample No.	Rock Type	$\delta^{18}O_{cpx}$ Meas.	$\delta^{18}O_{cpx}$ Calc.	$\delta^{18}O_{ol}$ Meas.	$^{87}Sr/^{86}Sr$ TIMS	2SE ppm	$^{143}Nd/^{144}Nd$ MC-ICP-MS	2SE ppm	$^{176}Hf/^{177}Hf$ MC-ICP-MS	2SE ppm	$^{206}Pb/^{204}Pb$ MC-ICP-MS	2SE	$^{207}Pb/^{204}Pb$ MC-ICP-MS	2SE	$^{208}Pb/^{204}Pb$ MC-ICP-MS	2SE
Mutnovsky																
N72	B				0.703327	10	0.513047	18	0.283197	8	18.375	0.0031	15.512	0.0031	38.151	0.0031
N75	B				0.703333	10	0.513062	16	0.283253	10	18.357	0.0027	15.505	0.0029	38.117	0.0029
N73	B		5.44	4.94	0.703363	10	0.513070	24	0.283239	14	18.374	0.0031	15.511	0.0030	38.148	0.0033
N71	B				0.703307	9	0.513071	20	0.283220	10	18.372	0.0027	15.512	0.0027	38.148	0.0028
N74	B		5.48	4.98	0.703336	10	0.513063	22	0.283258	9	18.376	0.0025	15.512	0.0028	38.153	0.0028
N79	BA				0.703228	8	0.513059	16	0.283268	11	18.344	0.0025	15.503	0.0027	38.102	0.0026
N94	B				0.703318	8	0.513080	20	0.283274	8	18.375	0.0021	15.512	0.0022	38.148	0.0022
N78	BA				0.703237	10	0.513062	18	—	—	18.357	0.0024	15.508	0.0025	38.126	0.0024
N98	BA				0.703335	10	0.513070	20	—		18.363	0.0027	15.505	0.0029	38.123	0.0027
N77	A				0.703302	9	0.513070	14	0.283254	10	18.372	0.0031	15.511	0.0031	38.145	0.0031
Gorely																
N69	B				0.703164	9	0.513043	18	0.283214	11	18.341	0.0024	15.502	0.0025	38.091	0.0024
N87	BA	5.35			0.703231	9	0.513049	16	0.283212	9	18.347	0.0025	15.503	0.0026	38.102	0.0025
N89	BA	5.13			0.703234	8	0.513040	16	0.283203	10	18.343	0.0027	15.502	0.0028	38.096	0.0028
N88	BA				0.703282	8	0.513034	16	0.283214	11	18.346	0.0028	15.505	0.0031	38.108	0.0029
N67	BA				0.703236	7	0.513057	14	0.283198	10	18.349	0.0029	15.504	0.0028	38.107	0.0028
N84	BA	5.28			0.703228	8	0.513057	14	0.283203	9	18.346	0.0027	15.503	0.0028	38.103	0.0027
N55	BA	5.31			0.703211	9	0.513049	14	0.283217	10	18.346	0.0030	15.503	0.0032	38.104	0.0031
N90	BA				—	—	0.513055	14	0.283211	13	18.348	0.0028	15.504	0.0029	38.106	0.0028
N80	BA				0.703208	8	0.513066	12	0.283211	10	18.348	0.0027	15.505	0.0034	38.107	0.0039
N60	TA				0.703234	9	0.513062	14	0.283202	10	18.348	0.0028	15.504	0.0029	38.106	0.0028
N86	TA				0.703231	8	0.513042	16	0.283208	10	18.350	0.0031	15.505	0.0038	38.110	0.0045
N82	T				—	—	0.513049	14	0.283213	9	18.347	0.0024	15.505	0.0024	38.105	0.0026
N58	R				0.703271	10	0.513059	14	0.283203	9	18.339	0.0027	15.503	0.0031	38.095	0.0031
K-AOC					TIMS		TIMS				TIMS		TIMS		TIMS	
881	AM				0.702430	5	0.513249	2	—	—	17.988	0.0010	15.3792	0.0010	37.311	0.0030
6539-4	AM				0.703851	5	0.513187	1	—		18.224	0.0030	15.4157	0.0030	37.612	0.0070
D210-1	AM				0.703477	5	0.513160	2	—	—	18.289	0.0020	15.3974	0.0020	37.598	0.0050

Abbreviations: B, basalt; BA, basaltic andesite; A, andesite; TA, trachyandesite; T, trachyte; R, rhyolite; AM, altered MORB.

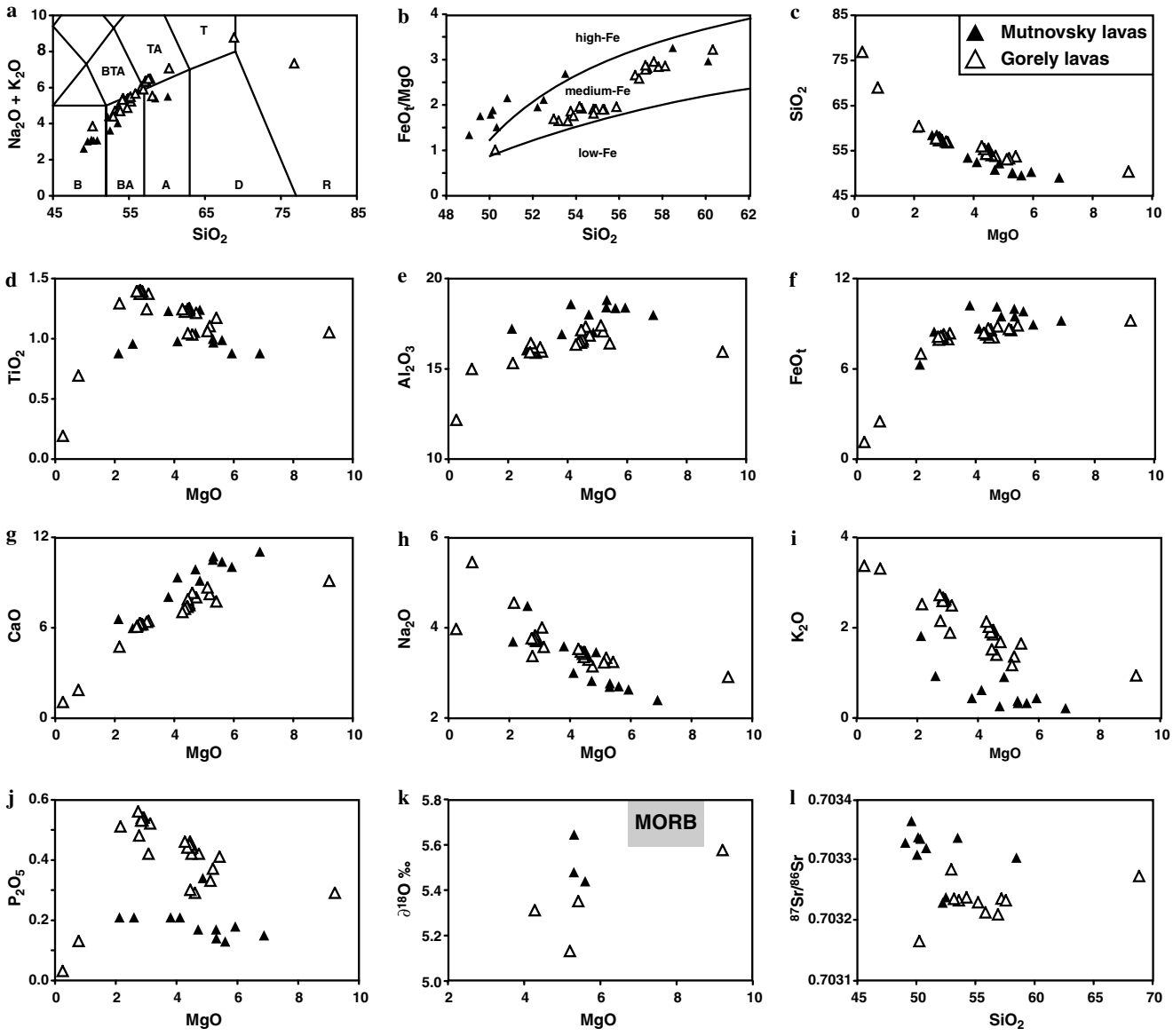

Fig. 2. Major and minor element and O–Sr-isotope composition of Mutnovsky (VF) and Gorely (RA) lavas ranging from basalt to rhyolite illustrating the role of fractional crystallisation and crustal contamination. Data sources are: Subdivision lines in the TAS and SiO_2 vs. FeO/MgO diagrams (a and b) (Le Maitre et al., 1989; Arculus, 2003), MORB (Sun and McDonough, 1989; Harmon and Hoefs, 1995). Abbreviations in the TAS diagram (a) are: B, basalt; BA, basaltic andesite; A, andesite; D, dacite; R, rhyolite; BTA, basaltic trachyandesite; TA, trachyandesite; T, trachyte.

ment concentrations mostly similar to or higher than normal mid-ocean ridge basalts (N-MORB) (Fig. 4). Mutnovsky and Gorely lavas generally show an enrichment of fluid-mobile elements (e.g., Cs, Tl, Rb, Ba, W, U, K, Pb, Sr, Sb and Li) relative to those that are less fluid-mobile or immobile (e.g., Th, Nb, Ta, REE, Mo, P, Sn, Zr, Hf, Ti and Y) although Gorely lavas exhibit higher concentrations in both fluid-mobile and -immobile elements. Basaltic lavas (basalts and basaltic andesites) from Mutnovsky generally have higher or more variable inter-element ratios in which the element in the numerator is more fluid-mobile than that in the denominator despite similar incompatibilities in basaltic melts during partial melting and fractional crystallisation, e.g., Cs/Th ($M = 0.13$–0.40, $G = 0.12$–0.27), Rb/Th ($M = 11.5$–18.1, $G = 12.4$–13.8), Ba/Th ($M = 385$–744, $G = 190$–306), U/Th ($M = 0.42$–0.56, $G = 0.38$–0.41), Pb/Ce ($M = 0.18$–0.32, $G = 0.16$–0.20), Sr/Nd ($M = 25$–50, $G = 14$–29) (Fig. 3). As to less fluid-mobile or -immobile elements, Mutnovsky lavas have lower inter-element ratios than Gorely lavas, e.g., Th/Nb ($M = 0.21$–0.41, $G = 0.36$–0.50), Th/Hf ($M = 0.15$–0.34, $G = 0.42$–0.55), La/Yb ($M = 1.6$–3.5, $G = 4.4$–4.8), Zr/Hf ($M = 31.2$–38.3, $G = 38.8$–40.7), Hf/Yb ($M = 0.61$–0.93, $G = 1.1$–1.4). Mafic Mutnovsky lavas have negative anomalies for Zr and Hf ($Zr/Zr^* = 0.58$–0.79, $Hf/Hf^* = 0.69$–0.81) $[Zr/Zr^* = Zr_{Nch}/(Nd_{Nch}^{2/4} * Sm_{Nch}^{2/4}), Hf/Hf^* = Hf_{Nch}/(Nd_{Nch}^{1/4} * Sm_{Nch}^{3/4})]$, and weak negative Ti-anomalies, whereas most Gorely lavas have less pronounced

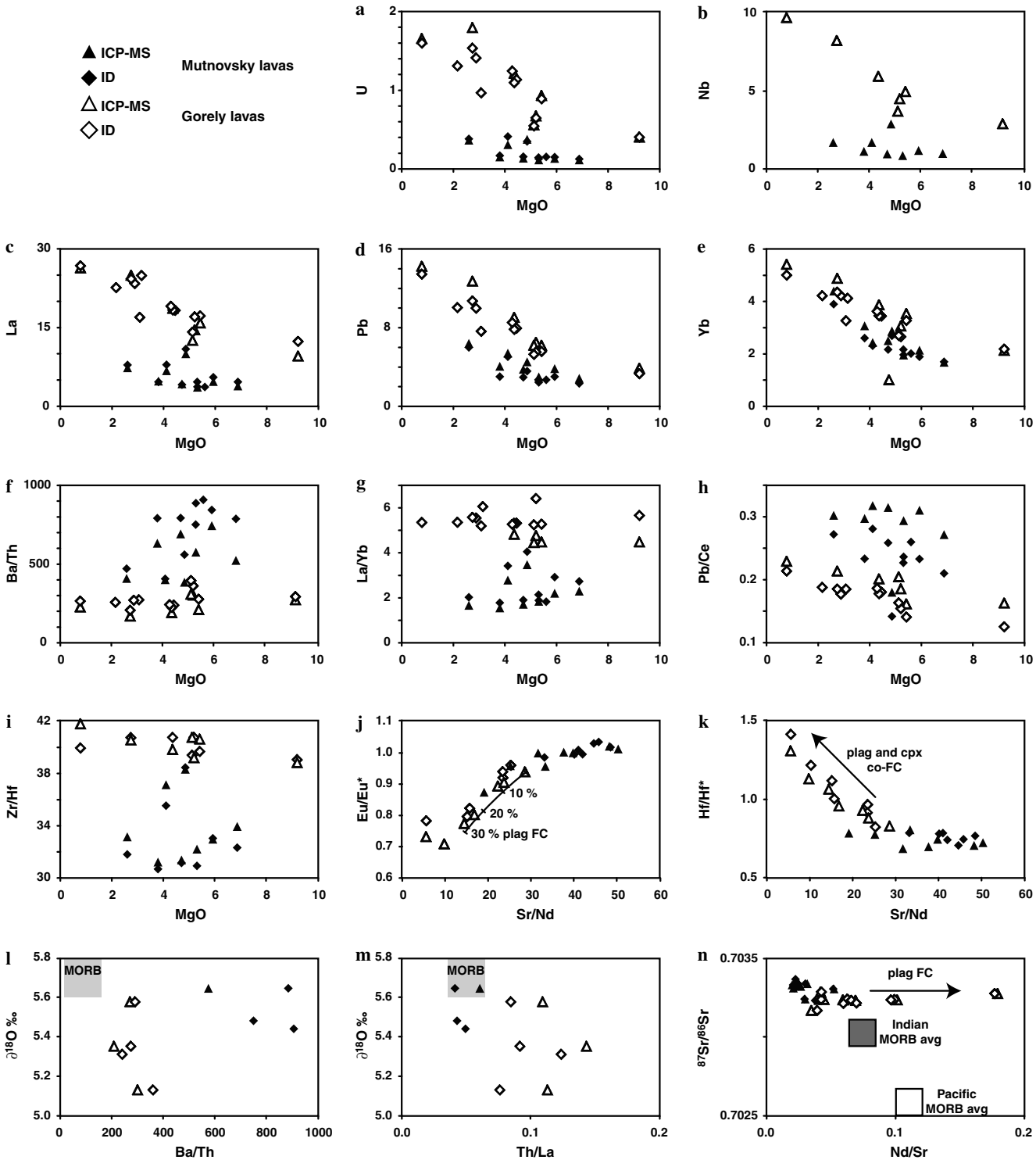

Fig. 3. Trace element and O–Sr-isotope composition of lavas from the Mutnovsky (VF) and Gorely (RA) volcanic centres displaying their systematic geochemical differences and the role of fractional crystallisation and crustal contamination. Rayleigh fractional crystallisation curve in (j) exhibits the effect of plagioclase removal on Eu-anomalies and Sr/Nd ratios for Gorely lavas using the most mafic sample N69 as starting composition. Calculation of Eu- and Hf-anomalies: $Eu/Eu^{*} = Eu_{Nch}/(Sm_{Nch} \times Gd_{Nch})^{1/2}$, $Hf/Hf^{*} = Hf_{Nch}/(Nd_{Nch}^{1/4} \times Sm_{Nch}^{3/4})$ (which includes Pm and Zr in the extended REE diagram), subscript Nch refers to "normalised to C1 chondrite". Data sources are: MORB (Sun and McDonough, 1989; Harmon and Hoefs, 1995), Indian and Pacific MORB averages (GEOROC Data Base georoc.mpch-mainz.gwdg.de), C1 chondrite (Sun and McDonough, 1989), partition coefficients for Rayleigh fractional crystallisation (McKenzie and O'Nions, 1991; McKenzie and O'Nions, 1995).

Zr–Hf-anomalies ranging from slightly negative to positive ($Zr/Zr^* = 0.83–1.07$, $Hf/Hf^* = 0.83–1.06$) and strong negative Ti-anomalies (Fig. 4). Correlations of Zr–Hf-anomalies with Eu-anomalies, Sr/Nd and Sc as observed for Gorely (but not for Mutnovsky) lavas (e.g., Fig. 3j and k) strongly suggest that Zr/Zr^* and Hf/Hf^* above 0.83 (i.e., higher than for the most mafic sample N69) result from combined plagioclase and clinopyroxene fractional crystallisation.

3.2. Stable and radiogenic isotope data

Oxygen isotope ratios were determined for olivine (Mutnovsky, $n = 2$) and clinopyroxene (Gorely, $n = 3$) separates. $\delta^{18}O_{cpx}$ values can be calculated from $\delta^{18}O_{ol}$ by $\delta^{18}O_{cpx} = \delta^{18}O_{ol} + 0.5‰$ assuming a melt temperature of ~1200 °C (Eiler, 2001). The measured $\delta^{18}O_{ol}$ of the two Mutnovsky samples (4.94‰ and 4.98‰) thus correspond to $\delta^{18}O_{cpx}$ of 5.44‰ and 5.48‰, which is slightly lower than the range of $\delta^{18}O$ reported for glass (5.57–6.43‰) from Mutnovsky basalts to andesites (Bindeman et al., 2004). The measured $\delta^{18}O_{cpx}$ of the three Gorely samples (5.13–5.35‰) are slightly higher than $\delta^{18}O_{cpx}$ (4.44‰) reported for a dacite from Gorely (Bindeman et al., 2004). The Mutnovsky and Gorely $\delta^{18}O_{cpx}$ thus tend to be slightly lower than MORB (5.7 ± 0.2) (Harmon and Hoefs, 1995) (Figs. 2k, 3l and m).

As to radiogenic isotope ratios Mutnovsky basalts to andesites tend to have higher $^{87}Sr/^{86}Sr$ and $^{143}Nd/^{144}Nd$ ratios (0.703228–0.703363; 0.513047–0.513080) than Gorely basaltic andesites to rhyolite (0.703208–0.703282; 0.513034–0.513066) (Fig. 5a). The Sr-isotope ratios of Mutnovsky and Gorely lavas are significantly higher than Pacific and Indian MORB glass samples, while the Nd-isotope ratios, however, fall between the averages for Pacific and Indian MORB. As illustrated in Fig. 5b, most Mutnovsky lavas have higher $^{176}Hf/^{177}Hf$ ratios (0.283197–0.283274) than Gorely lavas (0.283198–0.283217) that have a more homogenous Hf-isotopic composition. In the Nd–Hf-isotope space, the samples from both volcanic centres plot above the averages for both Indian and Pacific MORB but within the Indian MORB field (Fig. 5b).

In the uranogenic and thorogenic Pb-isotope diagrams most Mutnovsky basalts to andesites have higher Pb-isotope ratios ($^{206}Pb/^{204}Pb = 18.344–18.376$, $^{207}Pb/^{204}Pb = 15.503–15.512$, $^{208}Pb/^{204}Pb = 38.102–38.153$) than Gorely basalts to rhyolites that exhibit a much narrower range in Pb-isotopic composition ($^{206}Pb/^{204}Pb = 18.339–18.350$, $^{207}Pb/^{204}Pb = 15.502–15.505$, $^{208}Pb/^{204}Pb = 38.095–38.110$) (Fig. 6a–f). Despite the very limited range in $^{206}Pb/^{204}Pb$ (18.34–18.38) and the large range in major and trace element contents, the Pb-isotope ratios of Mutnovsky and Gorely form a remarkably well-defined positive correlation above but slightly steeper than the Northern Hemisphere Reference Line (NHRL) with r^2 better than 0.91 and 0.98, respectively (henceforth MG-array defined by the basaltic samples). The samples fall within the field for Indian MORB glass and plot above the field for Pacific MORB glass in the thorogenic Pb-isotope diagram (Fig. 6b). $^{206}Pb/^{204}Pb$ ratios do not correlate well with O–Sr–Nd–Hf-isotope ratios but Mutnovsky samples with the highest $^{206}Pb/^{204}Pb$ ratios also tend to have the highest $^{87}Sr/^{86}Sr$ and $^{143}Nd/^{144}Nd$.

4. Discussion

4.1. Crustal contamination

In order to examine the role of crustal contamination in the petrogenesis of the Kamchatkan arc lavas, we analysed the trace element and isotopic composition of the samples covering a large range in major element concentrations (e.g., $SiO_2 = 49.1–76.8$ wt% and $MgO = 0.3–9.2$ wt%) ranging from basalt to rhyolite. Despite their large variation in major and trace element concentrations and inter-element ratios Mutnovsky and Gorely lavas only show a very restricted range of O–Sr–Nd–Hf–Pb-isotopic compositions (Figs. 2–6). Oxygen isotope ratios tend to be lower than MORB (Figs. 2k, 3l and m), which may result from limited O-exchange with a low-$\delta^{18}O$ component in the course of near-surface processes related to the last glaciation of Kamchatka (e.g., involving meteoric water) or by re-melting of hydrothermally altered igneous crust (Bindeman et al., 2004). However, the absence of correlations between oxygen isotope ratios and major and trace elements and inter-element ratios (e.g., Figs. 2k, l and 3l, m) reflect that the budgets of major and trace elements and their radiogenic isotope ratios were not altered to a detectable level and therefore significant re-melting of altered basement material is very unlikely. This is consistent with the most evolved samples [(trachy-)andesites, trachytes and rhyolites] having Sr–Nd–Hf–Pb-isotopic compositions almost indistinguishable from the mafic lavas of the same volcanic centre (Table 4) and Sr–Nd–Hf-isotope ratios showing no correlations with major and trace elements and their ratios (e.g., Figs. 2l and 3n).

The Mutnovsky and Gorely samples form well-defined arrays in Pb-isotope diagrams (Fig. 6), for which the goodness-of-fit value of the linear regression is slightly better when non-basaltic samples are excluded. During substantial crustal assimilation it is impossible to maintain such a well-defined array subparallel to the NHRL with VF basalts having more radiogenic compositions than the RA basalts. However, since evolved samples appear to introduce some minor scatter to the Pb-isotope array, slight assimilation of crustal material cannot conclusively be excluded for some of the more evolved lavas but is inferred to be negligible for the basaltic samples. Crustal contamination, however, is also unable to explain the systematic shift in basalt geochemistry from the VF to the neighbouring RA volcanoes as observed throughout Kamchatka and other Pacific subduction zones and therefore must reflect processes operating in the Earth's mantle.

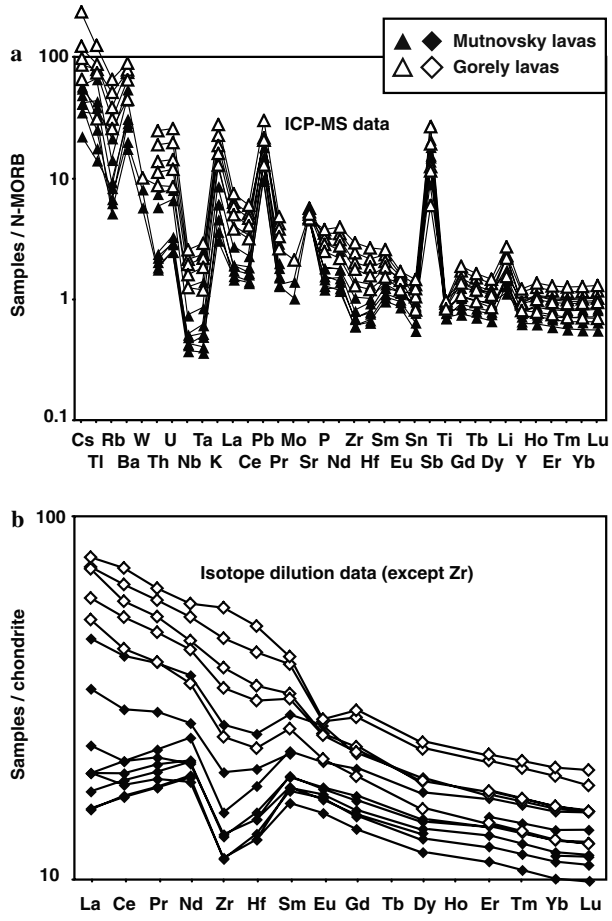

Fig. 4. Multi-element diagram with ICP-MS data normalised to N-MORB and Zr–Hf-extended rare earth element diagram with ID data (except Zr which is from XRF) normalised to C1 chondrite (Sun and McDonough, 1989) for Mutnovsky (VF) and Gorely (RA) basaltic samples. Pr concentrations in the ID REE diagram were calculated from linear interpolation of the normalised La and Nd contents.

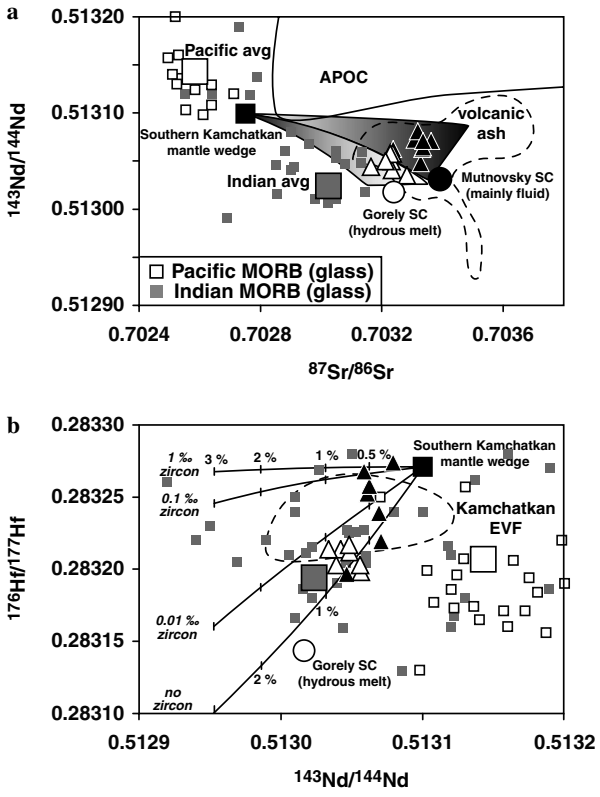

Fig. 5. Sr–Nd-isotope (a) and Nd–Hf-isotope (b) diagrams displaying the composition of basaltic lavas from Mutnovsky (VF) and Gorely (RA) and geochemical modelling results. Black and white circles denote the calculated Sr–Nd–Hf-isotopic composition of the Mutnovsky and Gorely slab components as outlined in the main text. Curves in the Nd–Hf-isotope diagram show mixing between the inferred Kamchatkan mantle wedge and eclogite-facies partial sediment melts (60% clinopyroxene and ~39% garnet) in the presence of residual monazite (0.01‰) and variable zircon contents (0–1‰ interpreted to reflect progressive zircon breakdown due to temperature-dependent increase of the zircon solubility with increasing slab surface depth. Note that in this scenario the Mutnovsky slab component composition is highly variable. Data sources are: Pacific and Indian MORB (Patchett and Tatsumoto, 1980; Patchett, 1983; Salters, 1996; Salters and White, 1998; Nowell et al., 1998; Vervoort et al., 1999; Chauvel and Blichert-Toft, 2001), Kamchatkan arc lavas from the eastern volcanic front (EVF) (Münker et al., 2004), volcanic ash drilled offshore the Izu Bonin and Kurile-Kamchatkan arcs (Cao et al., 1995; Schmidt, 2001), altered Pacific oceanic crust (APOC) (Hauff et al., 2003) (and this study), partition coefficients for batch partial metasediment melting (Tollstrup and Gill, 2005) and references therein), Kamchatkan subducted sediment column (KSSC) used as metasediment endmember as outlined in Appendix B, general mixing equation (Langmuir et al., 1978). Symbols are as in Fig. 2.

4.2. Mantle processes

4.2.1. The mantle wedge

Based on melt inclusion studies in olivine phenocrysts of Kamchatkan arc lavas, the mantle wedge beneath the Kamchatkan arc is relatively hot (~1275 °C at a pressure of ~1.5 GPa) and close to its dry solidus (Portnyagin et al., in press). These conditions are apparently due to mantle upwelling most likely caused by trench-upward mantle wedge corner flow and favour extensive partial melting in the presence of even small amounts of H_2O from hydrous fluids and melts in the spinel stability field in the Kamchatkan mantle (Portnyagin et al., in press). Under such circumstances hydrous phases such as phlogopite and amphibole are highly unlikely to be stable in the melting region of the Kamchatkan arc magmas and, as none of the lavas appear to be boninites, there is no reason to assume that the mantle wedge peridotite has a strongly depleted, i.e., harzburgitic, composition. This is consistent with Mutnovsky and Gorely lavas showing largely the same range of near-chondritic (17.6) (Sun and McDonough, 1989) Nb/Ta ratios ($M = 14.7$–18.9, $G = 15.4$–18.4) that are only fractionated significantly towards lower values in the mantle wedge for extreme depletion (Class et al., 2000; Münker et al., 2004). Therefore, in the melting region beneath Mutnovsky and Gorely the mantle wedge most likely consists of spinel-facies lherzolite.

The concentrations of relatively fluid-immobile, incompatible elements are useful to examine the depletion or enrichment of a magma source. If normalised to fertile

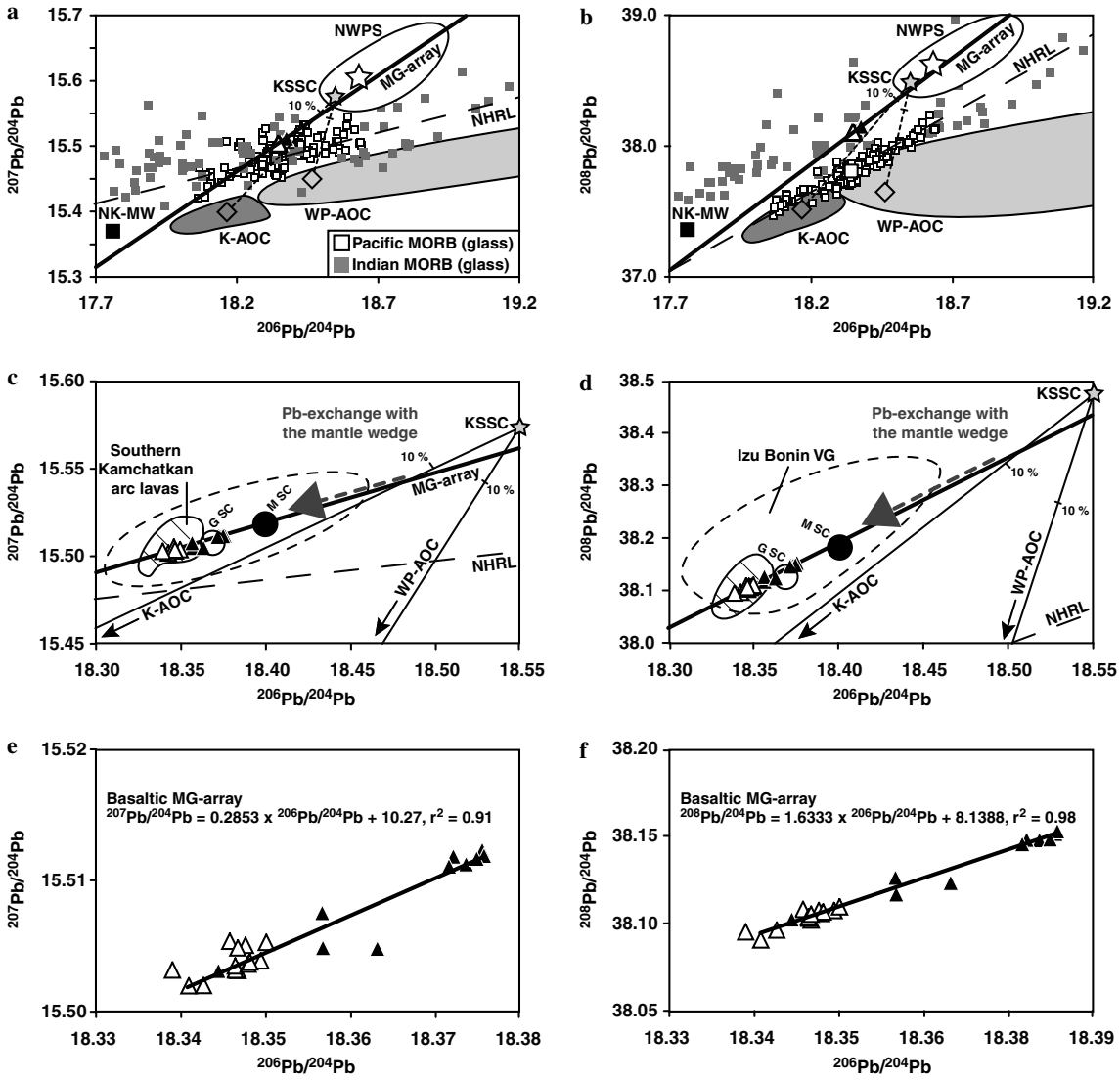

Fig. 6. Uranogenic (a, c, and e) and thorogenic (b, d, and f) Pb-isotope diagrams showing high-precision Pb (double-spike) isotope data of basalts to rhyolites from Mutnovsky (VF) and Gorely (RA) and relevant endmember reservoirs. The Mutnovsky-Gorely Pb-isotope array (MG-array) was calculated using the basaltic lavas (e and f). Black and white and circles display the composition of the Mutnovsky and Gorely slab components (M SC and G SC) calculated as outlined in the main text. Dashed lines in (c and d) with 10% tick marks are mixing lines between the estimated Kamchatkan subducted sediment column (KSSC) and altered oceanic crust (Kamchatkan (K-AOC) and western Pacific (WP-AOC), respectively). Data sources are: Pacific and Indian MORB glass data (GEOROC Data Base georoc.mpch-mainz.gwdg.de), northern Kamchatkan mantle wedge (NK-MW) (Portnyagin et al., 2005), northwestern Pacific sediments (NWPS, average denoted by white star) (clayey diatom oozes, claystones, nannofossil chalks, Mn-crusts) (McDermott and Hawkesworth, 1991; Kersting, 1995; Godfrey et al., 1997), Izu Bonin arc volcanogenic (VG) marine sediments (Schmidt, 2001), western Pacific altered oceanic crust (WP-AOC) (Hauff et al., 2003), southern Kamchatkan lavas (Kepezhinskas et al., 1997; Turner et al., 1998; Bindeman et al., 2004), Kamchatkan subducted sediment column (KSSC) as outlined in Appendix B, Northern Hemisphere Reference Line (NHRL) (Hart, 1984), general mixing equation (Langmuir et al., 1978). Symbols are as in Fig. 2.

MORB mantle (Pearce and Parkinson, 1993) (Fig. 7a), the patterns of Mutnovsky and Gorely lavas scatter around N-MORB but a systematic difference exists for the very highly to highly incompatible elements Nb, Zr, (Hf), Ti, Y and Yb. The range observed for the mafic Gorely lavas can partly be explained by substantial Rayleigh fractional crystallisation (Fig. 7a) but this process cannot account for the higher trace element levels of the most mafic Gorely lava (N69) compared to the mafic Mutnovsky samples with lower MgO contents.

The most mafic lavas from Mutnovsky fall slightly below N-MORB arguing that they were derived from a mildly depleted MORB-like mantle source. Ti, Y and Yb contents are a bit lower for Mutnovsky than for Gorely lavas suggesting that the mantle source beneath Mutnovsky is slightly more depleted than that beneath Gorely. This is consistent with Mutnovsky lavas plotting along a depletion trend in the Zr/Hf versus Lu/Hf diagram (Fig. 7b) and Zr/Hf ratios below N-MORB. The Mutnovsky samples are located at the low-Zr/Hf, high-Lu/Hf tip of the Indian and

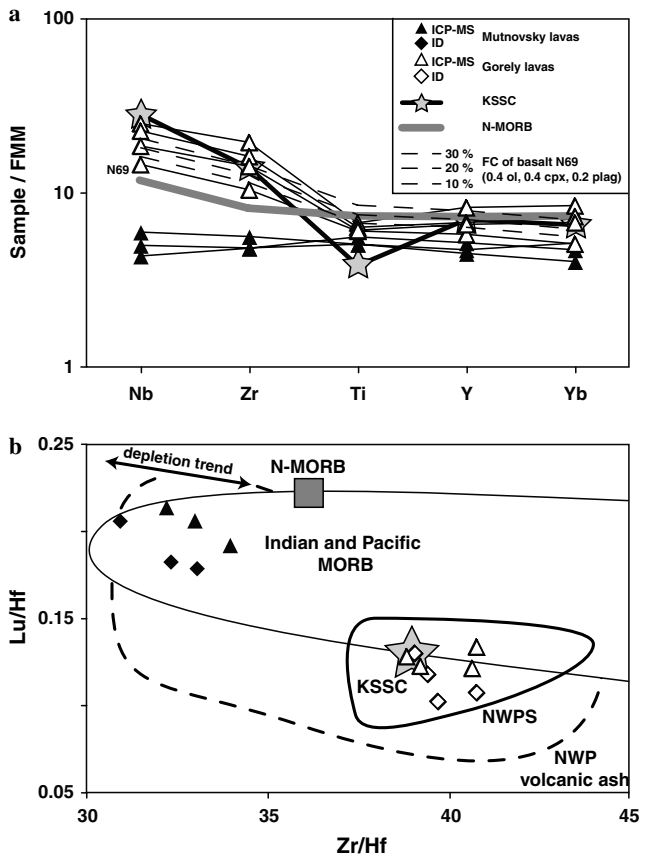

Fig. 7. Concentrations of very highly and highly incompatible elements Nb, Zr, Ti, Y and Yb normalised to fertile MORB mantle (FMM) (a) and Zr/Hf versus Lu/Hf diagram (b) showing the relatively fluid immobile element ICP-MS and ID composition of the most mafic Mutnovsky (VF) and Gorely (RA) lavas. Dashed lines in (a) display the effects of Rayleigh fractional crystallization for Gorely magmas using N69 as mafic endmember. Data sources are: FMM (Pearce and Parkinson, 1993), N-MORB (Sun and McDonough, 1989), Kamchatkan subducted sediment column (KSSC) as outlined in Appendix B, mineral-melt partition coefficients for trace elements used for Rayleigh fractional crystallisation calculations (McKenzie and O'Nions, 1991, 1995), Indian and Pacific MORB (GEOROC Data Base georoc.mpch-mainz.gwdg.de), northwestern Pacific volcanic ash (Cao et al., 1995), northwestern Pacific sediments (NWPS) (Bailey, 1993, 1996).

Pacific MORB field suggesting that the Zr, Hf and the HREE-budget of the mantle wedge beneath the VF was not significantly perturbed by the slab component consistent with what was proposed for the Kamchatkan VF based on a high-precision HFSE study (Münker et al., 2004).

The most mafic Gorely samples generally have normalised Ti, Y and Yb contents similar to or slightly below N-MORB and Nb and Zr concentrations above (Fig. 7a) coupled with elevated Zr/Hf and relatively low Lu/Hf (Fig. 7b). Lower Yb concentrations and Lu/Hf ratios may result from the retention of the HREE by residual garnet and high-pressure clinopyroxene for which the HREE are compatible on the spinel lherzolite solidus (Blundy et al., 1998; Münker et al., 2004). Melt inclusion studies of Mutnovsky and Gorely lavas infer melting in the spinel stability field (Portnyagin et al., 2005) indicating that lower Lu/Hf and generally higher element/Yb ratios of Gorely lavas (Figs. 3g, 4b and 7b) may either be due to higher proportions of high-pressure clinopyroxene and thus higher average melting depths in the mantle wedge (Blundy et al., 1998; Münker et al., 2004) or, alternatively, residual garnet in the source of the Gorely slab component. In the Zr/Hf versus Lu/Hf diagram, Gorely lavas plot within the field for northwestern Pacific sediments (NWPS), indicating that fluid-immobile inter-element ratios are not controlled by processes in the mantle wedge alone and may partly be due to the injection of a slab component capable of mobilising fluid-immobile elements. If this is correct, then the HFSE behaviour switches from conservative to non-conservative in the VF to RA transition, which may happen when slab-derived hydrous melts rather than fluids alone are involved in the production of the slab component (Pearce and Parkinson, 1993; Pearce and Peate, 1995).

4.2.2. Nature of the slab component(s)

Hydrous fluids and melts released from subducting oceanic lithosphere are main constituents of arc magmatism (Gill, 1981; Thorpe, 1982; Hawkesworth et al., 1993; Pearce and Peate, 1995; Stern, 2002). These slab components transport an array of fluid-mobile and fluid-immobile incompatible elements altering the mantle wedge composition from a MORB-type towards subduction zone geochemical signature. Inter-element ratios with fluid-mobile and -immobile elements are therefore particularly useful to elucidate whether an element behaves conservative or non-conservative and thus the nature of a slab component (e.g., fluid or melt) beneath a given volcanic centre. It was stressed recently that arc magmas inherit their Th/La and Th/Ce (and thus Th/Nd) from subducted sediments and it was estimated that ~30% of the Th in subducted sediments is recycled back to the crust with arc magmas (Hawkesworth et al., 1997; Plank, 2005). Sediment dehydration and melting experiments and comparison of mineral-melt and mineral-fluid partition coefficients argue that Th is more readily incorporated into silicate melts than hydrous fluids and therefore becomes mobile at the sediment solidus (Brenan et al., 1995; Johnson and Plank, 1999). Hence, Th/LREE ratios may constitute almost diagnostic inter-element ratios for distinguishing between hydrous fluid and melt involvement.

Compared to Gorely RA basaltic lavas, the Mutnovsky VF samples have lower Th/Nd and generally higher inter-element ratios in which the numerator element is more fluid-mobile than that in the denominator (e.g., Cs/Nb, Ba/Nb, Ba/Th, Pb/Nd, Pb/Ce, Sr/Nd and Sb/Nb) (Figs. 3f, h and 8). This strongly argues in favour of a slab component mainly consisting of hydrous fluid triggering extensive partial melting beneath the VF (Mutnovsky). Based on these inter-element ratios alone it cannot be distinguished whether the fluids stem from subducted northwestern Pacific sediments (NWPS) or AOC or any mixture thereof.

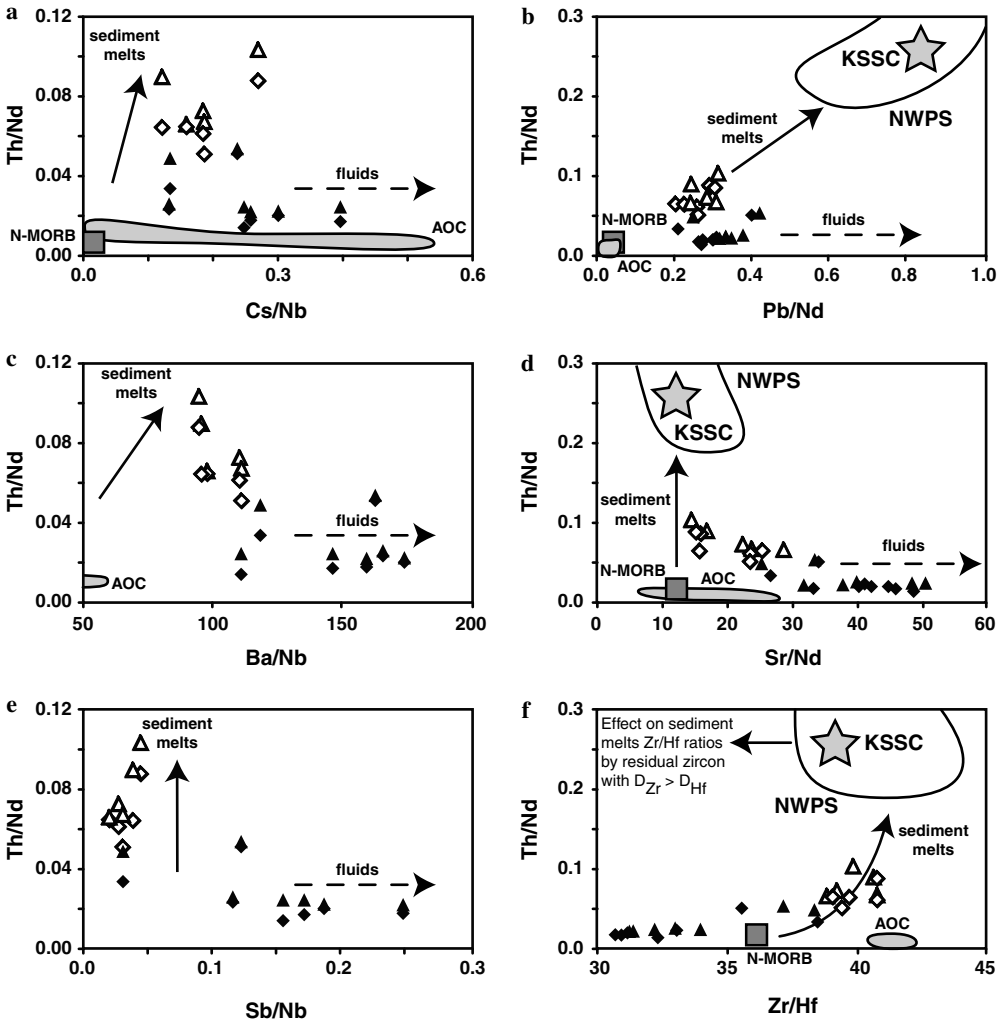

Fig. 8. Inter-element ratios with strongly fluid-mobile (Cs, Ba, Pb, Sr, and Sb) and less fluid-mobile or immobile elements (Nd, Nb, Zr, and Hf) illustrating the ICP-MS and ID composition of Mutnovsky (VF) and Gorely (RA) basaltic lavas and relevant endmembers such as MORB, Kamchatkan altered oceanic crust (K-AOC) and marine sediments. Data sources are: N-MORB (Sun and McDonough, 1989), northwestern Pacific sediments (NWPS) (Bailey, 1993, 1996), Kamchatkan subducted sediment column (KSSC) as outlined in Appendix B. Symbols are as in Fig. 6.

As illustrated in Fig. 8, Gorely RA lavas have elevated Th/Nd pointing to the recycling of incompatible elements from subducted sediments with hydrous melts. Elevated Th/Nd are generally coupled with relatively low Cs/Nb, Ba/Nb, Ba/Th, Pb/Nd, Pb/Ce, Sr/Nd, Sb/Nb and lower $^{143}Nd/^{144}Nd$ confirming that hydrous fluids alone are unable explain the geochemical composition of the Gorely RA lavas. Elevated Th/Nd are also linked to high Zr/Hf supporting the idea that subducted sediments are capable of altering the Zr/Hf ratios in the melting region of RA volcanoes as inferred in Fig. 7b. If this is correct, then the sediment melts were most likely generated in the absence of residual zircon in the metasediments since zircon has $D_{Zr}>D_{Hf}$ (Blundy and Wood, 2003; Tollstrup and Gill, 2005) and would therefore lead to melt Zr/Hf ratios lower than those of the bulk sediment composition (Fig. 8f).

Finally, it is worth noting that some basaltic Mutnovsky samples have an intermediate trace element composition between the group of mafic Mutnovsky samples with the lowest Th/Nd and Gorely volcanic rocks. The geochemical affinity of some of the Mutnovsky samples to Gorely lavas is independent of the degree of differentiation and may therefore indicate the occasional injection of a RA hydrous melt component to regions of the adjacent VF mantle source, probably caused by trench-ward mantle wedge corner flow.

4.2.3. Estimating the trace element compositions of the slab components

The trace element compositions of the slab components (hydrous fluids or fluid-melt mixture) in the Mutnovsky and Gorely magmas can be calculated with a simple two-component mass balance and by using adequate estimates for (1) the composition of their respective primary melts, (2) the composition of the mantle wedge and (3) the mass fraction of the slab component in the solid mantle prior to melting. The compositions of the Mutnovsky and Gorely primary melts were reversely modelled from the their

Table 5
Modelling endmembers and results for the slab component trace element and isotopic composition

	Kamchatkan	Bulk partition	Mutnovsky				Gorely			
	Mantle[a,d]	Coefficients[a]	Primitive melt[b]	Arc mantle	Slab input	Slab component for $X_{sc} = 1\%$[e]	Primitive melt[c]	Arc mantle	Slab input	Slab component For $X_{sc} = 1\%$[e]
	(ppm)		(ppm)	(ppm)	%	(ppm)	(ppm)	(ppm)	(%)	(ppm)
Rb	0.05	0.0001	2.55	0.46	89	40.7	12.65	1.31	96	126
Ba	0.563	0.00012	91.4	16.4	97	1581	249	25.7	98	2519
Th	0.0079	0.001	0.17	0.03	74	2.27	0.92	0.10	92	8.80
U	0.0032	0.0011	0.09	0.02	80	1.30	0.35	0.04	91	3.33
Nb	0.1485	0.0034	0.72	0.131	0	−1.61	2.54	0.270	45	12.3
Ta	0.0096	0.0034	0.04	0.007	0	−0.22	0.14	0.015	36	0.54
La	0.192	0.01	2.90	0.54	65	35.3	8.34	0.94	79	74.6
Ce	0.55	0.022	8.01	1.58	65	103	20.8	2.56	79	201
Pb	0.018	0.014	2.26	0.43	96	41.3	3.38	0.392	95	37.4
Nd	0.581	0.031	6.77	1.38	58	80.9	13.9	1.82	68	125
Sr	7.664	0.025	334	66.7	89	5912	398.26	50.1	85	4248
Sm	0.239	0.045	2.02	0.44	45	20.0	3.5	0.50	52	26.6
Zr	5.082	0.033	34.1	7.03	28	200	83.63	11.1	54	608
Hf	0.157	0.035	1.03	0.21	27	5.85	2.15	0.29	46	13.4
Eu	0.096	0.05	0.71	0.16	39	6.12	1.07	0.16	39	6.35
Gd	0.358	0.056	2.23	0.50	29	14.7	3.45	0.53	32	17.5
Dy	0.505	0.079	2.47	0.60	16	10.2	3.39	0.59	14	9.04
Y	3.328	0.088	14.4	3.63	8	33.1	19.65	3.58	7	28.6
Er	0.348	0.097	1.45	0.38	7	3.05	1.93	0.37	5	2.27
Yb	0.365	0.115	1.40	0.38	5	2.14	1.86	0.38	5	2.26
Lu	0.058	0.12	0.209	0.06	0	0.06	0.275	0.06	0	0.06
$^{87}Sr/^{86}Sr$	0.702750		0.703317			0.703390	0.703164			0.703238
$^{143}Nd/^{144}Nd$	0.513100		0.513059			0.513030	0.513043			0.513017
$^{176}Hf/^{177}Hf$	0.283275		0.283208			0.283031	0.283214			0.283143
$^{206}Pb/^{204}Pb$	17.760		18.374			18.400	18.341			18.369
$^{207}Pb/^{204}Pb$	15.370		15.512			15.518	15.502			15.508
$^{208}Pb/^{204}Pb$	37.360		38.150			38.184	38.091			38.126

See main text for details.

[a] Depleted MORB mantle trace element composition and bulk partition coefficients Irom Workman and Hart (2005).

[b] Average of primitive melts calculated from N71 and N72.

[c] Calculated from N69.

[d] Pb-isotopic composition from Portnyagin et al. (2005), Sr–Nd–Hf-isotopic composition estimates from the Sr–Nd–Hf-isotope diagrams in this paper.

[e] Mass fraction of the slab component in the solid mantle prior to melting.

most mafic lavas with the aid of Petrolog 2.0 (DanyuShevski, 2003) software by olivine addition until the melts where in equilibrium with Fo_{91} (Table 5). A recent estimate for average depleted MORB mantle (DMM) (Workman and Hart, 2005) provides constraints for the unmodified mantle wedge composition. Comprehensive O-isotope studies argue for a slab component contribution of ~1% to the magma source of most arc lavas (Eiler et al., 2000).

The slab component was then calculated using the equation:

$$[C^{i}_{SC}{}^{M,G} \cdot X_{SC} + C^{i}_{DMM} \cdot (1 - X_{SC})]/C^{i}_{prim.\ melt}{}^{M,G} = D^{i} + F^{M,G} \cdot (1 - D^{i}) (\text{solved for } C_{SC}{}^{M,G})$$

in which $C^{i}_{SC}{}^{M,G}$, C^{i}_{DMM} and $C^{i}_{prim.\ melt}{}^{M,G}$ are the concentrations of an element i in the slab component, depleted MORB mantle and the primary melts, respectively (M and G refer to the Mutnovsky and Gorely case, respectively). X_{SC} was assumed to be 1% based on the O-isotope studies of arc lavas (Eiler et al., 2000). D^{i} is the bulk partition coefficient of an element i for spinel-facies MORB mantle melting (Workman and Hart, 2005). The degrees of partial melting ($F^{M,G}$) beneath the Mutnovsky and Gorely volcanic centres were calculated from the Lu content of the estimated primary magma compositions using:

$$C^{Lu}{}_{DMM}/C^{Lu}_{prim.\ melt}{}^{M,G} = D^{Lu} + F^{M,G} \cdot (1 - D^{Lu}) \quad (\text{solved for } F^{M,G})$$

This equation can be derived from the previous one by assuming that Lu behaves perfectly conservative and there is no slab contribution (hence $X_{SC} = 0$) consistent with what was proposed for the behaviour of Lu in subduction zones (Münker et al., 2004). The approach suggests ~18% and ~10% degrees of partial melting for Mutnovsky and Gorely, respectively, which is largely consistent with relative differences in F inferred from melt inclusion studies (Portnyagin et al., in press). It is worth mentioning that the choice of the reference fluid-immobile element (e.g., Ti instead of Lu) does not significantly affect the results of the calculations. However, these data allow calculating the composition of the arc mantle prior to melting $[C^{i}_{ArcM}{}^{M,G} = C^{i}_{SC}{}^{M,G} \cdot X_{SC} + C^{i}{}_{DMM} \cdot (1 - X_{SC})]$ and from $C^{i}_{ArcM}{}^{M,G}$ and $C^{i}{}_{DMM}$ the slab input in percent. The results are reported in Table 5 and displayed in Fig. 9.

Based on these, major differences for the Mutnovsky and Gorely slab components (SC) are observed for the elements Rb, Th, U, Nb, Ta, the LREE and Zr, Hf (Fig. 9a) for which the Gorely SC shows significantly higher concentrations. The contents for the other trace elements, in particular for the strongly fluid-mobile ones (e.g., Ba, Pb and ±Sr), are fairly similar. However, in both cases the SC contributes with >50% to 98% to the Rb, Ba, Th, U, the LREE, Pb and Sr incompatible element budget of the arc magma source with concentrations reaching on the order of several hundred to several thousand times DMM (Fig. 9a and b). The Gorely SC also appears to have injected ~40–60% of the Nb, Ta, Zr and Hf to the RA melting region since the Gorely SC was calculated to have ~12 ppm Nb, ~0.5 ppm Ta, ~610 ppm Zr and ~13 ppm Hf (Table 5 and Fig. 9b). Together the data argue for a fluid-dominated origin of the Mutnovsky SC, eventually including minor proportions of a melt constituent. The latter is suggested by minor contents of Th, Zr, Hf (~2.3, ~200, ~5.8 ppm, respectively) although the enrichment of these elements is always relatively small compared to the nearest fluid-mobile element with similar incompatibility during mantle melting (Ba, U, Pb, and Sr). As to the Gorely SC significant proportions of a hydrous melt component have to be involved in order to explain the high and coupled mobility of fluid-mobile and fluid-immobile elements. The similarities in some of the most fluid-mobile element concentrations (Ba, Pb, and Sr) and the differences of the less fluid-mobile or fluid-immobile ones (Th, Nb, Ta, LREE, Zr, and Hf) suggest that a fluid-component similar to that in the Mutnovsky SC also plays a substantial role for the origin of the Gorely SC but is superimposed by an additional melt constituent. Such a mixed slab flux, composed of both hydrous fluids and sediment melts, was

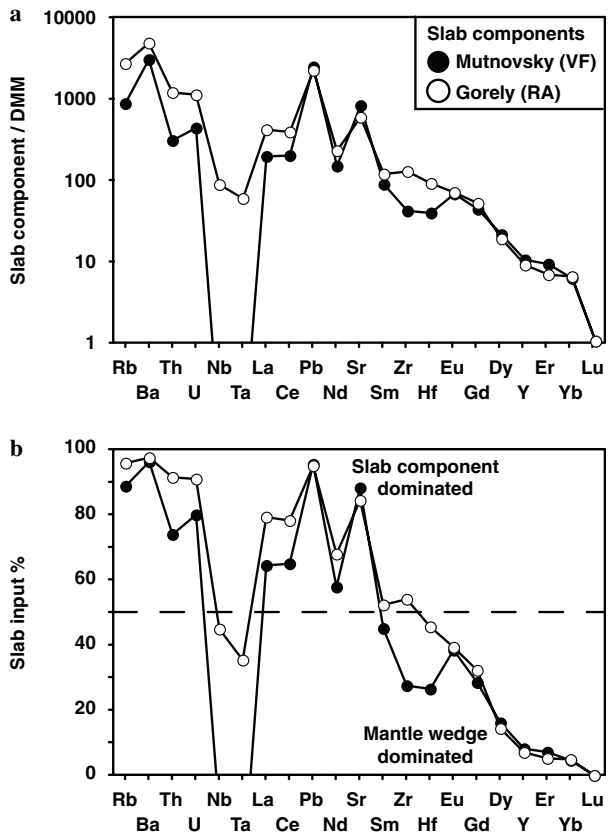

Fig. 9. Trace element composition of the Mutnovsky (VF) and Gorely (RA) slab components inferred from geochemical modelling including batch partial melting, mixing and mass balance equations as outlined in the main text. (a) Estimated incompatible element concentrations from Table 5 normalised to depleted MORB mantle (DMM), whereas (b) displays the slab input of individual elements in percent. Data sources are: DMM (Workman and Hart, 2005).

previously proposed for the Kurile RA (Ryan et al., 1995). Elevated Th/Nd strongly suggest that the melt constituent stems from subducted sediments (Fig. 8) but the presence of a background fluid from the AOC is possible and eventually even necessary to promote wet partial melting in the overlying sediment layer. However, sediment melting was previously suggested for the Aleutian, Kurile, Mariana and Tonga-Kermadec arcs (Ryan et al., 1995; Elliott et al., 1997; Turner et al., 1997; Class et al., 2000; George et al., 2005).

Notably, the slab component contribution of Nd, Sr and Pb are ~60–70%, ~85–90% and ~95–96%, respectively, indicating that the SC should have a major influence on the Nd-isotope ratios and strongly dominate the Sr–Pb-isotopic composition of the Mutnovsky VF and Gorely RA lavas. For Hf there exists a larger difference for the inferred SC contribution to the Mutnovsky and Gorely magma sources (~25% and ~50%, respectively).

4.2.4. Isotope compositions of the slab components

Assuming a simple two-component mass balance, only the mantle wedge and the slab component are governing the isotopic composition of the arc basalts and their mantle sources. The compositions of the Mutnovsky and Gorely slab components can be calculated using the following equation that is based on the general mixing equation (Langmuir et al., 1978):

$$R^{i}_{SC}{}^{M,G} = (R^{i}_{ArcM}{}^{M,G} - R^{i}_{KamM} \cdot (1 - X_{SC}) \cdot C^{i}_{DMM}/C^{i}_{ArcM}{}^{M,G}) / (X_{SC} \cdot C^{i}_{SC}{}^{M,G}/C^{i}_{ArcM}{}^{M,G}),$$

where R^{i} refers to the isotopic composition of the mixture (ArcM) and the respective endmembers (slab component, SC, and Kamchatkan mantle wedge, KamM) of a given element i. $R^{i}_{ArcM}{}^{M,G}$ is then identical to the isotopic composition of the Mutnovsky (average of N71 and N72) and Gorely (N69) lavas that were also used to calculate the trace element composition of the slab component. For R^{Pb}_{KamM} we chose the estimated Pb-isotopic ratios for the northern Kamchatkan mantle wedge (NK-MW in Fig. 6) (Portnyagin et al., 2005), whereas R^{Sr}_{KamM}, R^{Nd}_{KamM} and R^{Hf}_{KamM} where estimated from the systematics in the Sr–Nd- and Nd–Hf-isotope diagrams (Fig. 5).

As illustrated in Figs. 5 and 6, the differences of the Sr–Nd–Pb-isotopic compositions of the Mutnovsky and Gorely slab components are, naturally, comparable to the differences of the respective lavas. The Mutnovsky SC thus has higher $^{87}Sr/^{86}Sr$ and $^{143}Nd/^{144}Nd$ than the Gorely SC consistent with the injection of a SC dominated by hydrous fluids, and respectively, a SC containing substantial proportions of a melt component. However, the calculated Sr–Nd-isotopic compositions of the slab components depends on the choice of the isotopic composition of the mantle wedge, which so far is not very well constrained for Kamchatka. As indicated by Sr–Nd–Hf-isotope systematics, neither average Indian nor Pacific MORB constitute adequate end-members to explain the isotopic composition of all southern Kamchatkan lavas. For the Sr–Nd–Hf-isotope diagrams we therefore chose a mantle wedge composition consistent with the lava geochemistry of both the Kamchatkan and Izu Bonin subduction zones (including the Izu Bonin back-arc basin) (Taylor and Nesbitt, 1998; Pearce et al., 1999), thereby assuming that the mantle wedge composition is fairly similar for the western Pacific subduction zones. Better constraints are available in the Pb-isotope space. Here the slab components both fall on the well-defined MG-array in the Pb-isotope diagrams because the Kamchatkan mantle wedge composition (NK-MW), inferred independently from this study (Portnyagin et al., 2005), plots very close to the unradiogenic end of this array (Fig. 6a and b). Thus the Pb-isotope systematics strongly argue for a common origin of the radiogenic endmember in the volcanic front and rear-arc of Kamchatkan subduction zone, whereas the trace element systematics suggest different modes of element mobilisation (fluid versus melt) from the subducted oceanic lithosphere.

4.2.5. Provenance of the slab components

The uranogenic and thorogenic Pb-isotope arrays formed by the Mutnovsky and Gorely basaltic lavas only require two endmembers: (1) an unradiogenic reservoir such as the mantle wedge most likely represented by the NK-MW (Portnyagin et al., 2005) and (2) a radiogenic component. The latter can either be represented by subducted northwestern Pacific sediments or by a mixture of subducted sediments and altered oceanic crust. Notably, mixing lines between these two reservoirs intersect the MG-basalt Pb-isotope array (Fig. 6) suggesting that Pb comes both from sediments and AOC rather than from subducted sediments alone. The subducted sediment reservoir is here represented by the average Kamchatkan subducted sediment column (KSSC) composed of 70% northwestern Pacific sediments (NWPS) and 30% volcanic ash drilled offshore Kamchatka as outlined in Appendix B in order to take into account the accumulation of volcanic ash in the upper 150 m of the sediment pile. As AOC we consider both Kamchatkan altered oceanic crust (K-AOC) (Tables 2 and 4) and WP-AOC drilled offshore the Izu Bonin arc (Hauff et al., 2003) the former of which is more unradiogenic than the latter. The intersections of the KSSC-AOC mixing lines (assuming simple bulk mixing) with the MG-basalt array indicates on the order of 5–15% of the Pb coming from subducted sediments and the remainder from altered oceanic crust. These data along with weak negative Ce-anomalies (Ce/Ce^{*} down to 0.95) and the absence of a good correlation of Th/Nd with $^{143}Nd/^{144}Nd$ for Gorely lavas suggest that the sediment melt contribution to the slab component is, although significant, lower in the Kamchatkan than Mariana and Aleutian arcs (Hole et al., 1984; Elliott et al., 1997; Class et al., 2000).

The intersection of the KSSC-AOC mixing lines with the MG-array also provides an estimate of the Pb-isotopic composition of the slab component by the moment as it

leaves the slab surface (initial slab component, I-SC). Remarkably, the I-SC has considerably higher Pb-isotope ratios than the composition of the slab component in the melting regions (MR-SC) beneath the Mutnovsky and Gorely volcanic centres as inferred in the previous chapter. This discrepancy may arise from the exchange (or extraction) of fluid-mobile Pb of the mantle wedge with the I-SC as it rises towards the melting region (leaching of mantle wedge Pb) as was already proposed in the literature for Aleutian arc lavas (Miller et al., 1994). Graphically, in the Pb-isotope diagrams this process would result in a movement of the slab components downward along the MG-basalt array from the KSSC-AOC mixing lines towards the mantle wedge composition (indicated by grey arrows in Fig. 6c and d). Based on the geochemical study of Aleutian lavas the process can account for a substantial Pb-exchange on the order of 40% (Miller et al., 1994), a process that therefore may significantly and progressively alter the Pb-isotopic composition of the slab component within several tens of kilometres travel through the mantle wedge. However, if this process is capable of altering the Pb-budget of the SC to such an extent, then it may also to a similar level operate for all other strongly fluid-mobile elements (e.g., B, Li, U, and Sr) and eventually to some degree for the less fluid-mobile ones too (e.g., Th, Nd), which would have implications for the interpretations of their isotope ratios.

4.2.6. Temperature-dependent progressive break-down of zircon in subducted sediments?

The Mutnovsky lavas show a significantly larger Hf-isotope variation than Gorely lavas despite a similar range in Nd-isotope composition (Fig. 5b). From a first glance it might seem as if the unmodified mantle wedge has different Hf-isotopic compositions beneath Mutnovsky and Gorely, i.e., that the mantle wedge is, respectively, heterogenous and homogenous beneath these two volcanic centres. Considering their relatively small distance of ~15 km this is very unlikely and therefore it should be possible to provide a geochemical model assuming the same Nd–Hf-isotopic composition for the unmodified mantle wedge beneath both volcanic centres.

It was demonstrated recently that accessory residual phases such as zircon, rutile and monazite can have a strong influence on the Nd and Hf budget in partial metasediment melts and hence the curvature of mixing lines between MORB mantle and sediment melts (Tollstrup and Gill, 2005). As inferred above, the Mutnovsky and Gorely slab components involve minor and substantial amounts of a melt constituent, respectively. Therefore, the sediment melt constituent rather than the hydrous fluid in the slab component is likely to govern the Hf element budget and ultimately the resulting Hf-isotopic composition of the lavas.

Fig. 5b illustrates a set of mixing curves between a MORB-type mantle source and a sediment melt constituent from an eclogite-facies metasediment of KSSC bulk composition and accessory residual phases such as monazite and zircon. Rutile appears to be absent in the source of the Gorely SC since Nb and Ta are mobile and do not indicate fractionation (Table 5). Zircon is also unlikely to be a residual phase during generation of the metasediment melt involved in the petrogenesis of the Gorely lavas. This is inferred from their high Zr/Hf within the range of bulk NWPS (Fig. 7) and the fact that zircon has $D_{Zr}>D_{Hf}$ and therefore a metasediment melt coexisting with residual zircon should have lower Zr/Hf ratio than the zircon-bearing residue and the bulk sediment (Blundy and Dalton, 2000; Tollstrup and Gill, 2005) (Fig. 8f).

For the metasediments beneath the Mutnovsky and Gorely volcanic centres we assume different degrees of partial melting (1% and 10%, respectively) but the same proportion of monazite (0.01‰). It is worth noting that the curvature of the mixing lines and the position of their tick marks is primarily governed by the presence of the residual phases rather than the degree of partial melting. However, in our approach the amount of zircon was varied: For the source of the Mutnovsky slab component the zircon content decreases from 1‰ through 0.1‰ and 0.01‰ to 0‰ causing the 0.5–1% tick marks (indicating the mass fraction of the SC) to move progressively downwards through the Mutnovsky lava field (Fig. 5b). In other words, the Hf-isotopic composition of the Mutnovsky SC is variable and depends on the amount of zircon in the metasediment. However, it is worth noting that admixture of pure hydrous fluids with very low Hf/Nd ratio to the mantle wedge would yield convex-up mixing lines similar to those for metasediment melting with >0.1‰ zircon which could also explain the most radiogenic Hf-isotope ratios of the Mutnovsky VF lavas but not the least radiogenic $^{176}Hf/^{177}Hf$. The field of mafic Gorely lavas is intersected by the slightly convex-down mixing line calculated for the absence of residual zircon but the presence of trace amounts of monazite (0.01‰). The Mutnovsky and Gorely lava geochemistry and the geochemical modelling results suggest (progressive) break-down of zircon in the slab surface sediments during increasing slab surface depths for the VF to RA transition in the southern Kamchatkan arc. As pointed out by Tollstrup and Gill (2005) this would require slab surface temperatures high enough for sediments to melt but not too high (i.e., <~780 °C) to loose zircon as a residual phase. This is inferred from petrological experiments relevant for wet subducted slab surface metasediment melting beneath the VF to RA transition. These show that zircon solubility is strongly dependent on temperature and melt composition rather than pressure and that during partial melting of metacrustal material in a peraluminous granite system zircon solubility increases from ~100 ppm at 750 °C to ~1330 ppm at 1020 °C (Watson and Harrison, 1983).

In summary, our modelling results in the Nd–Hf-isotope diagram in combination with data from phase diagrams for metasediments (Schmidt and Poli, 2004) and calculations

for temperature-dependent zircon solubility (Watson and Harrison, 1983; Tollstrup and Gill, 2005) therefore indicate slab surface temperatures of ~700–780 °C beneath VF Mutnovsky and >780 °C beneath RA Gorely. Based on recent models for the thermal structure of active subduction zones (e.g., southern Kamchatka) this temperature increase may indeed be expected at the slab surface beneath the VF to RA transition (van Keken, 2003; Manea et al., 2005; Peacock et al., 2005).

4.2.7. Gorely melt components in Mutnovsky magmas but not vice versa

Mutnovsky lavas span a much wider range in Pb-isotope ratios than those from Gorely volcano (Fig. 6). Intriguingly, the mafic Mutnovsky lavas show correlations of Pb-isotope ratios with incompatible minor and trace element contents and inter-element ratios (Fig. 10). These correlations are restricted to the basaltic samples with MgO >4 wt. % for which $^{206}Pb/^{204}Pb$ systematically increases with decreasing Rb, Ba, K, P, Zr (XRF), Rb, Ba, Th, U, Nb, Ta, Zr, La, La, Ce, Pr, Nd, Hf (ICP-MS) and Rb, Ba, La, Ce, Nd, Pb, Hf (ID) concentrations ($r^2 \geqslant 0.7$). Numerous inter-element ratios (e.g., Rb/Sr, Rb/Hf, Ba/Sr, Ba/Yb, U/Th, Th/La, Th/Nd, Th/Hf, Th/Yb, Nb/Yb, Nb/La, K/Yb, ±Zr/Hf, Zr/Yb, Hf/Yb, Hf/Ti and Lu/Hf) also correlate with $^{206}Pb/^{204}Pb$ but, except for U/Th, correlate negatively. Hence the Mutnovsky and Gorely samples that have the lowest Pb-isotope ratios and thus lie closer to the NHRL also have the highest trace element concentrations and inter-element ratios. These systematics cannot result from crustal contamination.

The Mutnovsky lavas with the lowest $^{206}Pb/^{204}Pb$ have inter-element ratios approaching that of the mafic Gorely samples. Therefore, mixing curves were calculated using the average composition of the three most radiogenic Mutnovsky lavas with $^{206}Pb/^{204}Pb > 18.75$ and the most mafic Gorely lava with MgO > 9 wt%. These curves can adequately describe the correlations suggesting that Gorely melt components were admixed Mutnovsky ones but not vive versa. We interpret these Pb-isotope and trace element variations to reflect pollution of the Mutnovsky VF magma source with melts from the Gorely RA magma source caused by trench-ward mantle wedge corner flow. To our knowledge these are the first geochemical data that can

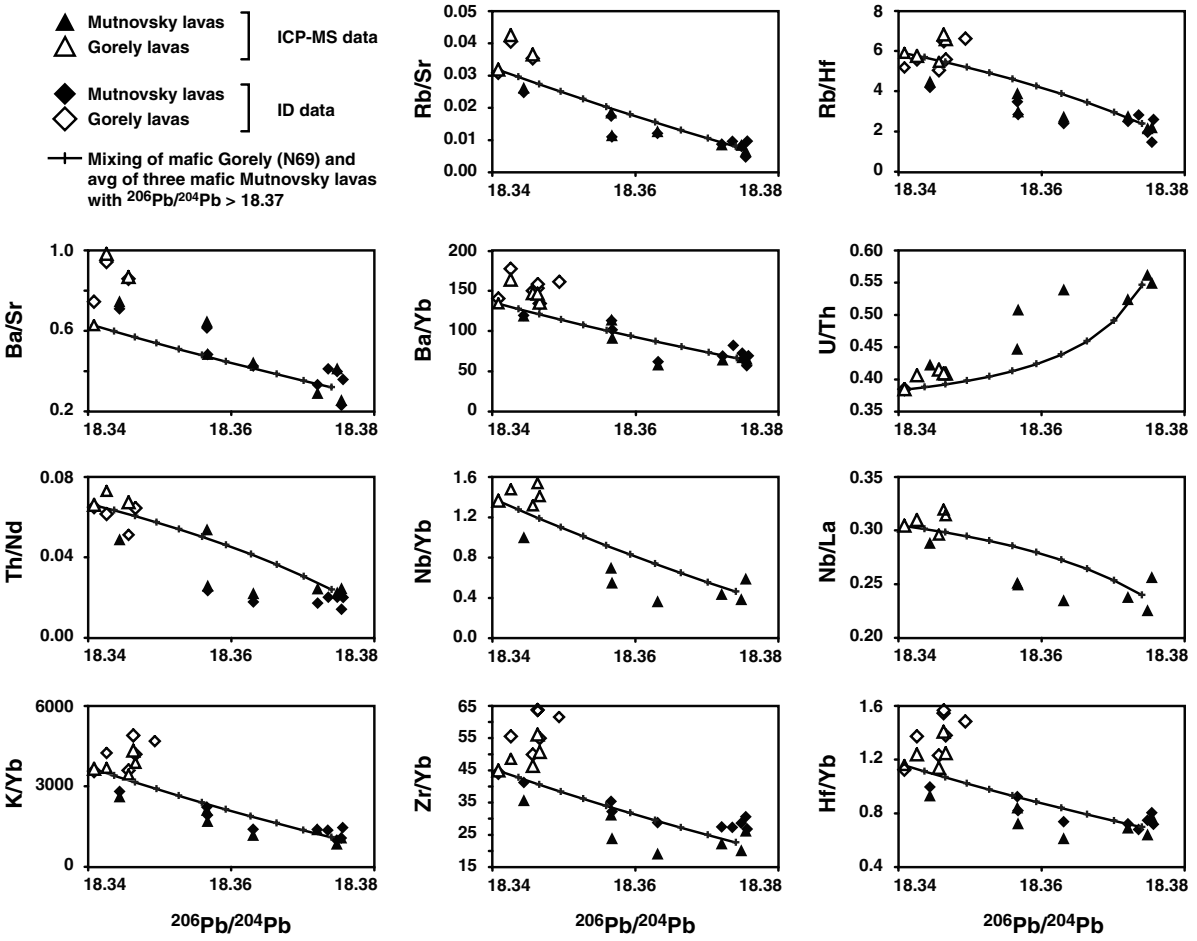

Fig. 10. Correlations of $^{206}Pb/^{204}Pb$ ratios with trace inter-element ratios for basaltic Mutnovsky (VF) lavas pointing to binary mixing between the most radiogenic Mutnovsky lavas ($^{206}Pb/^{204}Pb > 18.37$) and the most mafic sample from the Gorely (RA) volcanic centre (N69, MgO = 9.2 wt%). Tick marks on mixing curves denote 10% steps. Data sources are: General mixing equation (Langmuir et al., 1978).

directly describe this process with such a high resolution, i.e., for a pair of VF and RA volcanic centres located just 15 km apart (Fig. 1).

4.2.8. Geodynamic model inferred from the thermal structure of the southern Kamchatkan mantle wedge

A dynamic model displaying the thermal structure of and material transport in the southern Kamchatkan mantle wedge was recently presented in the literature (Manea et al., 2005). The model includes a strongly temperature-dependent mantle wedge viscosity that, in conjunction with some frictional heating at the interface between the subducted slab of oceanic lithosphere and the Kamchatkan lithosphere, leads to relatively high temperatures at the slab surface ample to promote sediment melting. As illustrated in Fig. 11, the 800 °C isotherm is predicted to be very close to the slab surface at depths <~100 km and appears to be touching or even crossing it at >100 km depth thereby producing conditions for wet sediment melting (Schmidt and Poli, 2004). Here, we should recall that the possible role of sediment melting in the origin of medium- to low-FeO/MgO (RA) and other high Ce/Yb lavas in subduction zone was already proposed more than two decades ago (Gill, 1981; Thorpe, 1982).

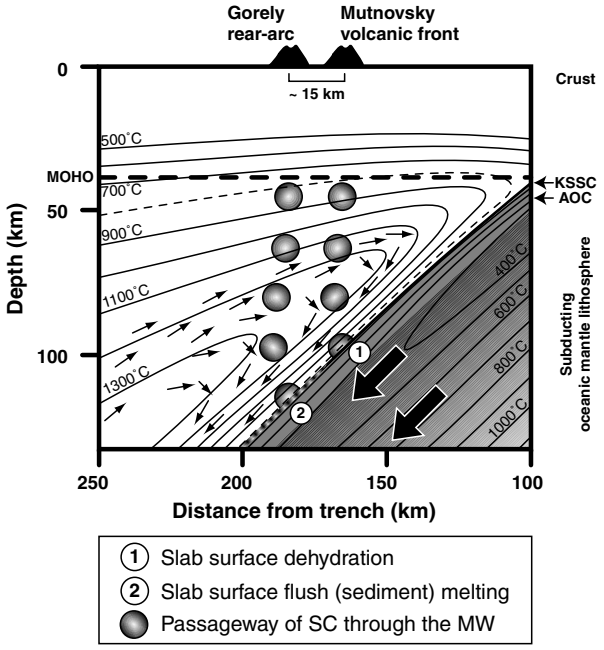

Fig. 11. Geodynamic model showing the thermal structure of the southern Kamchatkan subduction zone and near-vertical movement of larger blobs of mantle wedge material loaded with slab component through the mantle wedge based on the results from Manea et al. (2005) and the locations of the Mutnovsky (VF) and Gorely (RA) volcanoes. Wet metasediment (KSSC) melting is inferred for slab surface depths of 100–130 km, i.e., beneath the Gorely rear-arc volcano ②, whereas beneath the volcanic front the slab surface only dehydrates ①. During the transition from slab surface metasediment dehydration to partial melting the altered oceanic crust (AOC) is envisaged to continuously dehydrate providing the fluids for flush-melting. See main text for a detailed discussion.

According to the inferred thermal structure of the southern Kamchatkan subduction zone (Fig. 11), the sediments most likely pass the temperature range of 650–800 °C at depths <100 km, whereas the temperature of the underlying MORB layer (AOC) is ~100–200 °C lower. These P–T conditions meet the requirements for flush-melting of subducted sediments with the underlying and dehydrating MORB layer providing the required amounts of fluids through amphibole and chlorite decomposition reactions (Schmidt and Poli, 2004). At slab surface depths of >100 km temperatures of ~800 °C are then sufficient for wet metasediment melting according to the reaction phengite + jadeitic clinopyroxene + H_2O ⇒ melt. However, the wet solidus may be enhanced by ~100–200 °C if carbonates are present and in equilibrium with the fluid (Schmidt and Poli, 2004). It is therefore worth noting that the Kamchatkan subducted sediments are silica-rich and hence carbonate-poor due to high proportions of diatomaceous sediments and clays. Moreover, silicic volcanic ash layers and vitric shards dispersed in the biogenic and chemical sediments may further dilute carbonate in the subducted sediment column, in particular in the upper third of the northwestern Pacific sediment pile that accumulated dacitic to rhyolitic volcanic ash (see Appendix B for a summary of the stratigraphy). Therefore, the silica-rich sediments subducted beneath the Kamchatka are likely to be molten more readily than sediments in regions with high carbonate precipitation and only minor arc-derived volcanic ash production/deposition (e.g., immature island arcs).

The Mutnovsky and Gorely lava geochemistry and the location of the volcanic centres above the subducting slab is consistent with a transition from dehydration below the VF to partial melting of the slab surface under the RA. The thermal structure of the southern Kamchatkan mantle wedge and ultimately subducted oceanic lithosphere (Manea et al., 2005), the P–T conditions for metasediment and MORB dehydration/melting (Schmidt and Poli, 2004) as well as the Mutnovsky and Gorely lava chemistry provide constraints for the size, shape and location of the melting region. We propose that slab surface partial melting is restricted to a narrow zone within the metasediment layer beneath the rear-arc area (Gorely) with the onset of slab surface partial melting in the region of the volcanic front to rear-arc transition. While the slab surface sediments shift from dehydration to melting, the underlying layer of AOC dominantly only dehydrates providing aqueous fluids for flush-metasediment melting. Together, our geochemical study of Mutnovsky and Gorely lavas confirms the predictions of recent thermal models of active subduction zones which has implications for the understanding of the magma genesis and element cycling in subduction zones worldwide.

5. Conclusions

Major and trace element and O–Sr–Nd–Hf–Pb (double-spike) isotope analysis reveal a drastic across-arc shift in

the geochemical composition of mafic lavas from the volcanic front Mutnovsky and rear-arc Gorely volcanic centres in the active southern Kamchatkan subduction zone. Since the geochemical shift cannot be explained by fractional crystallisation and/or crustal contamination it has to result from differences in mantle processes beneath the two volcanic centres. The locations of the volcanoes indicate that the different processes operate in the vicinity of each other, viz. within ~15 km distance in the transition between the volcanic front to the rear-arc region where the slab surface depth increases from ~100 to ~120 km.

Based on the lava geochemistry, geochemical modelling and mass balance calculations, the geochemical shift mainly results from a combination of two processes operating in the mantle wedge and at the slab surface. These are (1) a VF to RA decrease in degrees of partial melting in the mantle wedge in conjunction with (2) a VF to RA transition of the nature of the slab component. As to the latter we propose a shift from dominantly dehydration of subducted sediments and AOC beneath Mutnovsky (volcanic front) to wet partial melting of subducted sediments beneath Gorely (rear-arc). The VF slab component is inferred to be primarily a hydrous fluid eventually containing minor amounts of a silicate melt, whereas the RA slab component involves a hydrous silicate melt. Slab surface partial melting beneath the RA is interpreted to take place in a narrow zone within the metasediment layer that is underlain by dehydrating AOC providing hydrous fluids required for (flush-)melting.

Nd–Hf-isotope systematics indicate that the VF to RA transition of the slab component may be associated with progressive break-down of zircon in the melting metasediments which has a major influence on the Hf-isotopic composition of the VF lavas. Pb (double-spike)-isotope and trace element data provide geochemical evidence for the pollution of Mutnovsky volcanic front magmas with Gorely rear-arc melt components, most likely resulting from trench-ward mantle wedge corner flow.

The drastic shift in lava geochemistry and the transition from slab surface dehydration to melting within ~15 km across-arc confirms recent models for the thermal structure of active subduction zones predicting higher temperature at the slab surface than hitherto thought. This study implies that (flush-)sediment melting may operate at slab surface depths of 100–130 km at least in subduction zones with moderate slab angles. Other wider implications of this paper are that there appears to be a higher likelihood for sediment melting in arc systems where the subducted sediment column is silicate-rich (carbonate-poor) due to high proportions of biogenic siliceous material and the accumulation of arc-derived, siliceous volcanic ash in the upper section of the subducting sediment column. "Arc cannibalism" should therefore be taken more seriously, e.g., as a process eventually having a considerable influence on the dehydration and melting behaviour of subducted sediments exposed at the slab surface and hence the element cycling in active subduction zones.

Acknowledgments

The analytical work was started at the Danish Lithosphere Centre (DLC) prior to its closure and continued at the Geological Institute. S.D. thanks Kirsten Bache, Joel Baker, Martin Bizzarro, Robert Frei, Hans-Christian Larsen, David Peate, Ole Stecher and Tod Waight for supporting the proposal for S.D.'s research fellowship and for an excellent start at the DLC and subsequently at the Geological Institute. Many thanks to Toby Leeper for assistance with TIMS Sr-isotope analysis and Maria Jankowski, Toni Larsen and Nadine Wittig for their help with the clean lab procedures in Copenhagen. Thanks go to Folkmar Hauff for Sr–Nd–Pb-isotope analysis of three K-AOC samples by TIMS, Dagmar Rau for XRF analysis and to Lasse Heuer for sample preparation at the IFM-GEOMAR in Kiel. We are grateful to N. Mironov, G. Avdeiko and O. Selyangin for support in the field. The manuscript was improved by conversations with Vera Ponomareva and helpful criticisms from two anonymous reviewers. S.D.'s research fellowship was funded by the Deutsche Forschungsgemeinschaft (DU426/1-1,2 and DU426/3-1) and the project in general by Danmarks Grundforskningsfond. Funding for field and analytical work and personnel for this study was also provided to KH and MP by the KOMEX II project (Bundesministerium für Bildung, Wissenschaft, Forschung und Technologie, BMBF) and SFB 574 "Volatiles and fluids in subduction zones" (this is contribution number 91).

Associate editor: Martin A. Menzies

Appendix A. Analytical techniques

A.1. Samples and sample preparation

Southern Kamchatkan volcanoes were accessed through joint German-Russian expeditions with cross-country vehicles and helicopters. Sample preparation was performed in the laboratories of the IFM-GEOMAR Leibniz Institute for Marine Sciences. The samples were crushed in a steel jaw crusher and sieved. Rock chips >1 mm were ground to fine powder in an agate mill and kept for major, trace and Sr–Nd–Hf-isotopic analysis. Rock chips in the 0.5–1 mm size fraction were cleaned ultrasonically in de-ionised water and used for Pb (double-spike)-isotopic analysis.

A.2. Major and trace element analysis

Whole rock geochemical analysis of major (Si, Ti, Al, Fe, Mn, Mg, Ca, Na and K) and selected trace elements (Co, Cr, Ni, V, Zn, Nb, Ga, Rb, Ba, Sr, Y and Zr) were performed on fused glass discs from 36 samples. Elemental concentrations were determined on a Philips X'unique PW 1480 X-ray fluorescence spectrometer (XRF) at the IFM-GEOMAR. International reference standards JB-2, JB-3 (basalts), JA-2, JA-3 (andesites), JR-2, JR-3 (rhyolites),

JG-2, GM (granites) and JF-1 (feldspar) were analysed along with the samples to evaluate analytical precision and accuracy. H_2O and CO_2 contents were determined using a Rosemont Infrared Photometer CSA 5003. The XRF major and trace element, H_2O and CO_2 data are reported in Table 1.

In addition, concentrations of an array of trace elements (Li, Sc, V, Cr, Co, Ni, Cu, Zn, Ga, Rb, Sr, Y, Zr, Nb, Mo, Sn, Sb, Cs, Ba, REE, Hf, Ta, W, Tl, Pb, Th and U) were measured on mixed acid (HF-aqua regia-$HClO_4$) pressure digests of 250 mg sample powder by inductively coupled plasma-mass spectrometry (ICP-MS) at the Institute of Geoscience, University of Kiel, using an Agilent 7500CS instrument. The precision of analytical results as estimated from duplicate sample measurements was better than 3% RSD. Details of the analytical procedure have been described in the literature (Garbe-Schönberg, 1993). Blanks and international standards, BE-N and BHVO-1, were analysed with the samples in order to evaluate the precision and accuracy of the measurements. The ICP-MS trace element data is presented in Table 2.

A.3. Chemical separation techniques

A.3.1. Isotope dilution analyses

High-precision measurements of Rb, Sr, Ba, REE, Hf, Pb, Th and U concentrations were performed on 22 samples by means of isotope dilution in the clean and ultra-clean laboratories of the Geological Institute at the University of Copenhagen. Samples were processed in two batches. For the determination of Rb, Sr, Ba and REE concentrations ca. 70 mg of whole rock powder was digested in a mixture of hot, concentrated HF-HNO_3. Following dissolution, samples were dried, converted to chloride form and completely dissolved in 6 M HCl. A 10% split was spiked with mixed ^{87}Rb–^{84}Sr, ^{135}Ba, and mixed LREE and mixed M-HREE isotopic tracers enriched in ^{138}La, ^{142}Ce, ^{145}Nd, ^{149}Sm, ^{153}Eu, ^{155}Gd, ^{161}Dy, ^{171}Yb, ^{166}Er and ^{176}Lu. The remaining, unspiked 90% aliquot was kept for chemical separation and isotopic analysis of Nd. After sample-spike homogenisation, evaporation and conversion to nitrate, Sr and Ba were extracted using Sr-Spec resin and 2 M HNO_3, 7 M HNO_3 and ultra-pure H_2O (Pin et al., 2003). The remaining matrix was passed over large AG50W-X8 cation exchange columns to separate Rb in 2 M HCl. REE were either collected in a M-HREE and a L-MREE fraction using 4 and 6 M HCl (Baker et al., 2004), or collected in bulk in 6 M HCl. The bulk REE fraction was further separated into M-HREE and L-MREE fractions using miniaturised columns loaded with 0.3 ml of RE-Spec resin and 3, 1 and 0.02 M HNO_3. For Pb, Th and U isotope dilution analyses, approximately 100 mg of rock chips were leached in cold 2 M HCl for 5–10 min to remove surface contamination and rinsed thoroughly in ultra-pure H_2O. The leached chips underwent complete dissolution in two digestion cycles using hot HF-HNO_3. After dry-down, the samples were converted to chloride form and dissolved in 6 M HCl. A 5–10% aliquot was spiked with a mixed ^{229}Th–^{236}U and a ^{206}Pb tracer. The Pb was then isolated from the matrix elements and U-Th using AG1-X8 anion exchange resin and 1 M HBr and purified with a second pass. U–Th was separated from the remaining matrix elements on small AG50W-X8 cation exchange resin using 7 M HNO_3, ultra-pure H_2O and 7 M HCl.

A.3.2. Isotope ratio analyses

Natural Sr-isotope ratios were determined on whole rock powders that were washed in hot 6 M HCl for 1 h prior to HF-HNO_3 dissolution. Sr was separated and purified by two passes on the Sr-Spec ion extraction resin with 3 M HNO_3 and H_2O.

Nd-isotope ratios were determined on the unspiked ~90% aliquot of the solution used for Rb–Sr–Ba–REE isotope dilution analysis (see above). Nd was separated in a two-step procedure, first separating a bulk REE fraction from matrix elements on AG50W-X8 cation exchange resin and using 2 M HCl, ultra-pure H_2O, 2 M HNO_3 (to elute Ba), ultra-pure H_2O and 6 M HCl. Nd was further separated from other REE using HDEHP resin and 0.25 M HCl.

Separation of Hf for isotopic analysis was achieved by flux assisted fusion and dissolution in 2 M HCl followed by cation exchange and extraction chromatographic separation as described in the literature (Ulfbeck et al., 2003).

Pb-isotope analysis was performed on ~100 mg of separated matrix chips that were acid washed with ~4 M HCl for 1 h on the hotplate and multiply rinsed with ultra-pure H_2O to remove anthropogenic Pb. The samples were digested in cleaned and capped Savillex PTFE beakers with a concentrated HF-HNO_3 mixture of blank tested SeaStar ultrapure acids in an ultra-clean Pb-laboratory. Following evaporation, conversion to chloride and dissolution in 1 M HBr, Pb was separated and purified by two passes on an anion exchange resin AG1-X8 100–200 mesh in a Class 100 laminar flow bench (Baker et al., 2004).

A.4. Mass spectrometry and data acquisition

For O isotope analysis at the Royal Holloway College, separates of olivine and clinopyroxene phenocrysts or fragments thereof were picked under the binocular microscope. About 1.7 mg ± 10% of each mineral separate or standard were weighed and loaded into a 16-hole nickel sample tray. Each tray contains up to 12 sample unknowns, whereas the other positions are occupied by standards. The tray is inserted into the reaction chamber and then evacuated and the oxygen is released by a 30W Synrad CO_2 laser in the presence of BrF_5 reagent. The oxygen yield is determined as a calibrated pressure based on the known or estimated oxygen content of the mineral being analysed. Accurate yield calculations are essential as low yields result in low $\delta^{18}O$ values for all mineral phases. For most minerals yields of >90% are required to give satisfactory $\delta^{18}O$ values and the oxygen gas is measured using a VG Isotech

(now GV Instruments) Optima dual inlet isotope ratio mass spectrometer (IRMS). Oxygen isotope values are reported relative to Vienna Standard Mean Ocean Water (V-SMOW) and the data obtained are calibrated using 2 standards, which are a widely distributed standard (GMG II (Gore Mountain garnet)), supplied by Prof. J. Valley of the University of Wisconsin, reported value of 5.7‰) and an internal standard (San Carlos Olivine (SC OL)), which has a $\delta^{18}O$ value of 4.88‰ determined over 10 years of analysis. Both standards are in turn calibrated against an international standard (NBS-30 biotite, known value of +5.1‰ relative to V-SMOW). Based on the standard values, for each run a small constant correction, normally less than 0.5‰, is applied to the data. This offset is caused by variations in quality of the BrF_5 reagent and the performance of the KBr scrubber and molecular sieve O_2 trap. Overall the precision on replicate is reported as being better than ±0.1‰. The oxygen isotope data is reported in Table 4.

Isotope ratios of samples and sample-spike mixtures were measured by means of TIMS and MC-ICP-MS at the Geological Institute, University of Copenhagen. Sr samples were loaded on Re filaments with TaF_5 and dilute H_3PO_4 (sandwich loading technique) and run multi-dynamically on a VG 54 TIMS. During analysis, mass 85 was monitored to determine contributions from Rb on mass 87, and this was found to be insignificant ($^{87}Rb/(^{87}Rb + {}^{87}Sr) < 100$ ppm). Sr isotope ratios were exponentially mass bias corrected using $^{86}Sr/^{88}Sr = 0.1194$ as normalising ratio. All samples were analysed under the same operating conditions and interspersed with certified Sr standard NBS 987 yielding $^{87}Sr/^{86}Sr = 0.7102347 \pm 17$ (2SD, $n = 12$). Long-term reproducibility of $^{87}Sr/^{86}Sr$ for NBS 987 is reported to be 25 ppm. Measured Sr isotopic compositions and analytical uncertainties are reported in Table 4.

Isotopic analyses of Rb, Sr, Ba Hf, REE, Th and U separates for isotope dilution and of Nd, Hf and Pb for isotopic compositions were performed on an Axiom MC-ICP-MS in static acquisition mode at the Geological Institute, University of Copenhagen. All samples were introduced into the mass spectrometer as dry aerosols by means of a Cetac desolvating nebuliser operating at a typical uptake rate of 0.05–0.08 ml/min. Spiked Rb isotopic compositions were measured using Zr to monitor and correct for mass fractionation as described in the literature and Rb concentrations reproduce to better than 0.5% using this technique (Waight et al., 2002b). Sr concentrations were determined using sample-standard bracketing to correct for mass bias. Reproducibility of Sr concentrations using this method are reported to be <0.5% (Waight et al., 2002a,b). Spiked Ba isotopic compositions were determined by sample-standard bracketing methods using a collector array covering the mass array mass 135 to mass 140. This allowed for simultaneous acquisition of ^{135}Ba (spike isotope), ^{137}Ba and ^{138}Ba, while potential interferences from La and Ce (both on mass 138) were monitored at masses 139 and 140, respectively. Ba concentrations of international rock standards AGV-1, BCR-2 and JB-2 were determined for reference and agree within error with recommended values (Table 2). Reproducibility of Ba concentrations as evaluated by analysis of replicate samples digestions was better than 0.2%. REE ID analyses were carried out as described in the literature yielding reproducibilities of 1% on concentration measurements and 0.2% on inter-element ratios (Baker et al., 2002). The ID data are reported in Table 3.

Hf isotopic analyses were carried out following a published procedure (Bizzarro et al., 2003), and unknown samples were measured relative to an in-house Hf isotopic standard yielding $^{176}Hf/^{177}Hf = 0.281868 \pm 15$ (2 SD, $n = 11$) and adjusted to 0.281890 corresponding to $^{176}Hf/^{177}Hf = 0.28216$ obtained for JMC 475. Nd isotopic compositions were determined on bulk rock MREE-LREE fractions using methods as described in the literature (Luais et al., 1997). Nd isotopic ratios are reported relative to $^{143}Nd/^{144}Nd = 0.512105 \pm 12$ (2 SD, $n = 12$) obtained for a 200 ppb AMES Nd-standard solution and adjusted to 0.512130 which corresponds $^{143}Nd/^{144}Nd = 0.51186$ for La Jolla. Pb isotopic determinations were performed using the Pb double-spike technique described in the literature (Baker et al., 2004). Analytical procedure blanks for Pb were ⩽30 pg. Nd–Hf–Pb (double-spike) isotope data are reported in Table 4.

Appendix B. Estimating the average composition of the Kamchatkan subducted sediment column (KKSC)

B.1. Stratigraphy and lithology

Northwestern Pacific marine sediments were drilled and sampled on various cruises with research vessels (Bailey, 1993). Some studies focussed on the uppermost 5–15 m of the sediment column (Ninkovich and Robertson, 1975) whereas Deep Sea drilling projects recovered marine sediments from up to ~1 km depths reaching upper Eocene sediments (e.g., DSDP Leg 192 and ODP Leg 145, Sites 881 through 884) (Creager et al., 1973). The sediment pile due east of the Southern Kamchatkan trench, however, was estimated to be ~600 m thick (Ninkovich and Robertson, 1975). Based on the stratigraphy, there appears to be a marked difference in the abundance of volcanic ash layers throughout the sediment column with clearly higher proportions of volcanic ash in the upper 200 m (Pliocene to present) (Cao et al., 1995; Creager et al., 1973). This shift in stratigraphy, however, was not taken into account in studies aiming at providing constraints on the geochemical composition of the subducted sediment column for the Kamchatkan arc (Kersting, 1995; Plank and Langmuir, 1998).

In the upper section of the subducted sediment column (~150 m corresponding to Pliocene to Present), volcanic ash material is found in significant amounts (often ca. 5–20%) as glass-shards and igneous phenocrysts in glass-bearing and glass-rich diatomaceous clays and diatom oozes (Creager et al., 1973). Numerous volcanic ash layers are

embedded in these sediments (Creager et al., 1973; Ninkovich and Robertson, 1975; Cao et al., 1995) that mainly consist of vitric shards and microlites of clinopyroxene, Fe–Ti-oxides, plagioclase and quartz. Their thickness is generally on the centimetre to decimetre scale but several single ash layers were found to be 1–2.5 m thick (Ninkovich and Robertson, 1975; Cao et al., 1995). Based on the stratigraphy the proportion of the ash layers is estimated to be ca. 20–40% (Creager et al., 1973; Cao et al., 1995) but it may comprise up to ~80% in the uppermost 5–15 m section of the sediment columns (Ninkovich and Robertson, 1975). Based on these data, it can be estimated that volcanic ash in total comprise 25–45% of the upper section of the subducted sediment column.

The lower section (below the upper 150 m) is marked by a drastic decrease of the volcanic ash abundance. In this section, the proportion of volcanic ash in the marine sediments appears to be <5%. Volcanic ash reappear below the lower Oligocene but they are altered and partly or completely turned into palagonite and smectite (Cao et al., 1995). The volcanic ash layers in the upper and lowermost sections, however, have fundamentally different geochemical compositions; mainly dacitic to rhyolitic in the upper and basaltic andesitic in the lowermost section.

B.2. Inferred geochemical composition

A detailed geochemical study of the ash layers drilled along the Kamchatkan-Kurile trench shows that the ash were mainly derived from island arcs rather than hot-spots or mid-ocean ridges (Cao et al., 1995). The composition of the ash in the upper 150 m ranges from basaltic andesite to rhyolite but they fall mostly in the field for dacites to rhyolites, have multi-element patterns similar to arc lavas and generally show pronounced negative Eu-anomalies. Most of the ash have relatively low Sr-isotope (0.703131–0.704533) and high Nd-isotope (0.512933–0.513110) ratios very similar to the lavas from the adjacent Kurile-Kamchatkan island arc (Cao et al., 1995; Bailey, 1996; Kepezhinskas et al., 1997; Turner et al., 1998; Dorendorf et al., 2000; Churikova et al., 2001; Bindeman et al., 2004; Münker et al., 2004). Since the abundance of volcanic ash in northwestern Pacific marine sediments increases with decreasing distance from the trench, the bulk Sr-isotope ratios of sediments decrease from >0.7100 in the open ocean environment (dominated by pelagic sediments with upper crustal composition) to <0.7065 near the Kurile-Kamchatkan trench (Bailey, 1993) thereby approaching the Kurile and Kamchatkan island arc compositions ($^{87}Sr/^{86}Sr$ = 0.702761–0.706386 and 0.703180–0.703650, respectively). Interestingly, the Pb-isotope data provided for northwestern Pacific marine sediments are significantly more radiogenic ($^{206}Pb/^{204}Pb$ = 18.59–18.78) (Kersting, 1995) than most Kurile and Kamchatkan ($^{206}Pb/^{204}Pb$ = 18.198–18.043–18.389 and 18.485, respectively) arc lavas (Bailey, 1996; Kepezhinskas et al., 1997; Turner et al., 1998; Dorendorf et al., 2000; Churikova et al., 2001; Bindeman et al., 2004; Münker et al., 2004; GEOROC, 2005) (and this study). The analysed Pacific sediments are clayey diatom oozes, claystones and nannofossil chalks and were all sampled between 156 and 800 m below seafloor in the section of the sediment column in which volcanic ash are scarce. Therefore, the Pb-isotope data of Kersting (1995) can only represent a part of and certainly not the entire sediment column subducted beneath Kamchatka in contrast to what is proposed in the literature (Plank and Langmuir, 1998). Pb- and Hf-isotope data of volcanic ash from northwestern Pacific sediments are not available in the literature but, because the volcanic ash embedded in the upper section northwestern Pacific sediments primarily have dacitic and rhyolitic compositions and Sr–Nd-isotope ratios within the range of igneous rocks in the Kurile-Kamchatkan arcs, they can be inferred from the Pb–Hf-isotopic composition of the andesites, dacites and rhyolites outcropping onshore in the arcs.

In order to provide an estimate of the mean composition of the Kamchatkan subducted sediment column (KSSC), we used the calculated average compositions of the north-

Table 6
Estimated compositions of northwestern Pacific maiine sediments without volcanic ash layers (NWPS), volcanic ash layers and Kamchatkan subducted sediment column (KSSC) as outlined in Appendix B

	NWPS (only includes dispersed ash)	Volcanic ash layers	KSSC (30% ash layers)
Rb	59.2	55.3	58.0
Ba	993	530	854
Th	4.77	3.80	4.48
U	2.20	1.47	1.98
Nb	6.27	3.96	5.58
K	19426	20626	19786
La	15.4	13.4	14.8
Ce	33.8	31.5	33.2
Pb	14.3	14.1	14.2
Pr		4.36	—
Sr	215	194	209
Nd	16.6	18.6	17.2
Sm	3.71	4.73	4.02
Zr	115	156	127
Hf	2.86	4.21	3.26
Eu	0.99	1.27	1.07
Ti	4163	3511	3967
Gd		5.26	—
Tb	0.66	0.88	0.73
Dy		5.59	—
Li	31.7	—	—
Y	23.4	37.5	27.6
Ho	—	1.24	—
Er		3.48	—
Tm	—	0.55	—
Yb	2.26	3.78	2.71
Lu	0.33	0.61	0.41
$^{87}Sr/^{86}Sr$	0.706771	0.703552	0.705873
$^{143}Nd/^{144}Nd$	0.512635	0.513033	0.512764
$^{176}Hf/^{177}Hf$	0.283000	0.283223	0.283086
$^{206}Pb/^{204}Pb$	18.631	18.359	18.550
$^{207}Pb/^{204}Pb$	15.603	15.505	15.574
$^{208}Pb/^{204}Pb$	38.619	38.125	38.473

western Pacific sediments that do not include discrete volcanic ash layers (NWPS) and the average composition of the drilled volcanic ash layers based on the data available in the literature (Table 6). The major and trace element and Sr–Nd–Pb-isotopic composition of the NWPS was calculated from the geometric mean of data for sediments collected on different cruises in the northwestern Pacific (Vulcano, Rama, DSPD and ODP) ($n = 50$) (Bailey, 1993; Kersting, 1995; Bailey, 1996; Bindeman et al., 2004). Since the Pb-isotope ratio of the NWPS endmember is similar to pelagic sediments and Mn-crusts, the average Hf-isotope ratio was adjusted to 0.2830 considering the given average Nd-isotope ratio of 0.512635 to make the Nd–Hf-isotope composition fall at the radiogenic edge of the field for pelagic sediments and Mn-crusts in the Nd–Hf-isotope diagram. The average major and trace element and Sr–Nd-isotopic composition of the volcanic ash was calculated from the geometric mean of the volcanic ash data ($n = 124$) provided by Cao et al. (1995). The Pb–Hf-isotopic composition was inferred from the composition of andesites through rhyolites in the Kurile-Kamchatkan arc ($n = 27$ and 12, respectively) (Bailey, 1996; Kepezhinskas et al., 1997; Turner et al., 1998; Dorendorf et al., 2000; Churikova et al., 2001; Bindeman et al., 2004; Münker et al., 2004; GEOROC, 2005 and this study). The NWPS endmember was mixed with the volcanic ash average in proportions of 70:30 (Table 6) as based on the stratigraphy and referred to as the Kamchatkan subducted sediment column (KSSC).

References

Arculus, R.J., 2003. Use and abuse of the terms calcalkaline and calcalcalic. *J. Petrol.* **44** (5), 929–935.

Bailey, J.C., 1993. Geochemical history of sediments in the northwestern Pacific Ocean. *Geochem. J.* **27**, 71–90.

Bailey, J.C., 1996. Role of subducted sediments in the genesis of Kurile-Kamchatka island arc basalts: Sr isotopic and elemental evidence. *Geochem. J.* **30**, 289–321.

Bailey, J.C., Larsen, O., Frolova, I., 1987. Strontium isotope variation in lower Tertiary–Quaternary volcanic rocks from the Kurile island arc. *Contrib. Mineral. Petrol.* **95**, 155–165.

Baker, J., Waight, T., Ulfbeck, D., 2002. Rapid and highly reproducible analysis of rare earth elements by multi collector inductively coupled plasma mass spectrometry. *Geochim. Cosmochim. Acta* **66** (20), 3635–3646.

Baker, J., Peate, D.W., Waight, T., Meyzen, C., 2004. Pb isotopic analysis of standards and samples using a ^{207}Pb–^{204}Pb double spike and thallium to correct for mass bias with a double-focussing MC-ICP-MS. *Chem. Geol.* **211**, 275–303.

Bindeman, I.N., Ponomareva, V.V., Bailey, J.C., Valley, J.W., 2004. Volcanic arc of Kamchatka: a province with high-∂18O magma sources and large-scale $^{18}O/^{16}O$ depletion of the upper crust. *Geochim. Cosmochim. Acta* **68** (4), 841–865.

Bizzarro, M., Baker, J.A., Ulfbeck, D., 2003. A new digestion and chemical separation technique for rapid and highly reproducible determination of Lu/Hf and Hf isotope ratios in geological materials by MC-ICP-MS. *Geostandards Newslett. J. Geostandards Geoanal.* **27**, 133–145.

Blundy, J., Dalton, J., 2000. Experimental comparison of trace element partitioning between clinopyroxene and melt in carbonate and silicate systems, and implications for mantle metasomatism. *Contrib. Mineral. Petrol.* **139**, 356–371.

Blundy, J.D., Wood, B.J., 2003. Partitioning of trace elements between crystals and melts. *Earth Planet. Sci. Lett.* **210**, 383–397.

Blundy, J.D., Robinson, J.A.C., Wood, B.J., 1998. Heavy REE are compatible in clinopyroxene on the spinel lherzolite solidus. *Earth Planet. Sci. Lett.* **160**, 493–504.

Brenan, J.M., Shaw, H.F., Ryerson, F.J., Phinney, D.L., 1995. Mineral-aqueous fluid partitioning of trace elements at 900 °C and 2.0 GPa: constraints on the trace element chemistry of mantle and deep crustal fluids. *Geochim. Cosmochim. Acta* **59**, 3331–3350.

Cao L.-Q., Arculus R.J., McKelvey B.C., 1995. Geochemistry and petrology of volcanic ashes recovered from Sites 881 through 884: A temporal record of Kamchatka and Kurile volcanism. In: Rea, D.K., Scholl, D.W., Allan, J.F. (Eds.), *Proceedings of the Ocean Drilling Program 145*, Scientific Results, vol. 145, pp. 345–381.

Chauvel, C., Blichert-Toft, J., 2001. A hafnium isotope and trace element perspective on melting of the depleted mantle. *Earth Planet. Sci. Lett.* **190**, 137–151.

Churikova, T., Dorendorf, F., Worner, G., 2001. Sources and fluids in the mantle wedge below Kamchatka, evidence from across-arc geochemical variation. *J. Petrol.* **42** (8), 1567–1593.

Class C., Miller D., Goldstein S.L., Langmuir C.H., 2000. Distinguishing melt and fluid subduction components in Umnak volcanics, *Aleutian Arc. Geochemistry, Geophysics, Geosystems 1*, Paper number 1999GC000010.

Creager J.S., Scholl D.W., party a. s. s., 1973. Initial Reports of the Deep Sea Drilling Project. U.S. Government Printing Office.

Danyushevski, L., 2003. Petrolog 2.x software, Available from: <www.geol.utas.edu.au/~leonid/Petrolog.html>.

Dorendorf, F., Wiechert, U., Wörner, G., 2000. Hydrated sub-arc mantle: a source for the Kluchevskoy volcano, Kamtchatka/Russia. *Earth Planet. Sci. Lett.* **175**, 69–86.

Eiler, J.M., 2001. Oxygen isotope variations of basaltic lavas and upper mantle rocks. In: Valley, J.W., Cole, D.R. (Eds.), *Stable Isotope Geochemistry*, Vol. 43. Mineralogical Society of America, pp. 319–364.

Eiler, J., Crawford, A., Elliott, T., Farley, K.A., Valley, J.V., Stolper, E.M., 2000. Oxygen isotope geochemistry of oceanic-arc lavas. *J. Petrol.* **41** (2), 239–256.

Elliott, T., Plank, T., Zindler, A., White, W., Bourdon, B., 1997. Element transport from slab to volcanic front at the Mariana arc. *J. Geophys. Res.* **102** (B7), 14991–15019.

Fedotov S.A., Masurenkov Y.P., 1991. Active volcanoes of Kamchatka. Nauka.

Garbe-Schönberg, C.D., 1993. Simultaneous determination of thirty-seven trace elements in twenty-eight international rock standards by ICP-MS. *Geostandard Newslett.* **17** (1), 81–97.

George, R., Turner, S., Morris, J., Plank, T., Hawkesworth, C., Ryan, J., 2005. Pressure–temperature–time paths of sediment recycling beneath the Tonga-Kermadec arc. *Earth Planet. Sci. Lett.* **223**, 195–211.

GEOROC, 2005. Geochemistry of Rocks of the Oceans and Continents. MPI für Chemie, Mainz, Germany.

Gill, J., 1981. *Orogenic Andesites and Plate Tectonics*. Springer Verlag.

Godfrey, L.V., Lee, D.-C., Sangrey, W.F., Halliday, A.N., Salters, V.J.M., hein, J.R., White, W.M., 1997. The Hf isotopic composition of ferromanganese nodules and crusts and hydrothermal manganese deposits: implications for seawater Hf. *Earth Planet. Sci. Lett.* **151**, 91–105.

Gorbatov, A., Kostoglodov, V., Suarez, G., Gordeev, E., 1997. Seismicity and structure of the Kamchatka subduction zone. *J. Geophys. Res.* **102** (B8), 17883–17898.

Gorbatov, A., Domiguez, J., Suarez, G., Kostoglodov, V., Gordeev, E., 1999. Tomographic imaging of the P-wave velocity structure beneath the Kamchatka pensinsula. *J. Geophys. Res.* **137**, 269–279.

Harmon, R.S., Hoefs, J., 1995. Oxygen isotope heterogeneity of the mantle deduced from global 18O systematics of basalts from different geotectonic settings. *Contrib. Mineral. Petrol.* **120**, 95–114.

Hart, S.R., 1984. A large-scale isotope anomaly in the Southern Hemisphere mantle. *Nature* **309**, 753–757.

Hauff, F., Hoernle, K., Schmidt, A., 2003. Sr–Nd–Pb composition of Mesozoic Pacific oceanic crust (Site 1149 and 801, ODP Leg 185): Implications for alteration of ocean crust and the input into the Izu-Bonin-Mariana subduction system. *Geochem. Geophys. Geosystems* **4** (8).

Hawkesworth, C.J., 1982. Isotope characteristics of magmas erupted along destructive plate margins. In: Thorpe, R.S. (Ed.), *Andesites: Orogenic Andesites and Related Rocks*. John Wiley and Sons, pp. 549–574.

Hawkesworth, C.J., Gallagher, K., Hergt, J.M., McDermott, F., 1993. Mantle and slab contributions in arc magmas. *Annu. Rev. Earth Planet. Sci.* **21**, 175–204.

Hawkesworth, C.J., Turner, S.P., McDermott, F., Peate, D.W., van Calsteren, P., 1997. U–Th isotopes in arc magmas: implications for element transfer from the subducted crust. *Science* **276**, 551–555.

Hochstaedter, A.G., Kepezhinskas, P., Defant, M., Drummond, M., Koloskov, A., 1996. Insights into the volcanic arc mantle wedge from magnesian lavas from the Kamchatka arc. *J. Geophys. Res. Solid Earth* **101** (B1), 697–712.

Hochstaedter A., Gill J., Peters R., Broughton P., Holden P., 2001. Across-arc geochemical trends in the Izu-Bonin arc: Contributions from the subducting slab. *Geochemistry Geophysics Geosystems 2*, Paper number 2000GC000105.

Hole, M.J., Saunders, A.D., Marriner, G.F., Tarney, J., 1984. Subduction of pelagic sediments: implications for the origin of Ce-anomalous basalts from the Mariana Islands. *J. Geol. Soc. Lond.* **141**, 453–472.

Ishikawa, T., Nakamura, E., 1994. Origin of the slab component in arc lavas from across-arc variation of B and Pb isotopes. *Nature* **370**, 205–208.

Ishikawa, T., Tera, F., 1997. Source, composition and distribution of the fluid in the Kurile mantle wedge: constraints from across-arc variations of B/Nb and B isotopes. *Earth Planet. Sci. Lett.* **152**, 123–138.

Ishikawa, T., Tera, F., Nakazawa, T., 2001. Boron isotope and trace element systematics of three volcanic zones in the Kamtchatka arc. *Geochim. Cosmochim. Acta* **65** (24), 4523–4537.

Johnson, M.C., Plank, T., 1999. Dehydration and melting experiments constrain the fate of subducted sediments. *Geochemistry Geophysics Geosystems 1*, Paper number 1999GC000014.

Kelemen, P.B., Hanghøj, K., Greene, A.R., 2004. One view of the geochemistry of subduction-related magmatic arcs, with an emphasis on primitive andesite and lower crust. In: Rudnick, R.L. (Ed.), *The Crust*, Vol. 3. Elsevier Pergamon, pp. 593–659.

Kepezhinskas, P., McDermott, F., Defant, M.J., Hochstaedter, A., Drummond, M.S., Hawkesworth, C., Kolosov, A., Maury, R.C., Bellon, H., 1997. Trace element and Sr–Nd–Pb isotopic constraints on a three-component model of Kamtchatka arc petrogenesis. *Geochim. Cosmochim. Acta* **61** (577–600).

Kersting, A.B., 1995. Pb isotope ratios of North Pacific sediments, Sites 881, 883, and 884: Implications for sediment recycling in the Kamchatkan arc. In: Rea, D.K., Scholl, D.W., Allan J.F. (Eds.), *Proceedings of the Ocean Drilling Program 145*, Scientific Results, vol. 145, pp. 383–387.

Langmuir, C.H., Vocke, J.R.D., Hanson, G.N., Hart, S.R., 1978. A general mixing equation with applications to Icelandic basalts. *Earth Planet. Sci. Lett.* **37**, 380–392.

Le Maitre, R.W., Bateman, P., Dudek, A., Keller, J., Lameyre Le Bas, M.J., Sabine, P.A., Schmid, R., Sorensen, H., Streckeisen, A., Woolley, A.R., Zanettin, B., 1989. *Classification of igneous rocks and glossary of terms*. Blackwell.

Luais, B., Telouk, P., Albaréde, F., 1997. Precise and accurate neodymium isotopic measurements by plasma-source mass spectrometry. *Geochim. Cosmochim. Acta* **61** (22), 4847–4854.

Manea, V.C., Manea, M., Kostoglodov, V., Sewell, G., 2005. Thermal models, magma transport and velocity anomaly estimation beneath Southern Kamchatka (Chapter 31). In: Foulger, G.R., Anderson, D.L., Natland, J.H., Presnall D.C. (Eds.), Plates, Plumes & Paradigms, vol. 388, Geological Society of America Special Paper, pp. 388–31.

McDermott, F., Hawkesworth, C., 1991. Th, Pb, and Sr isotope variations in young island arc volcanics and oceanic sediments. *Earth Planet. Sci. Lett.* **104**, 1–15.

McKenzie, D., O'Nions, R.K., 1991. Partial melt distributions from inversion of rare earth element concentrations. *J. Petrol.* **32** (5), 1021–1091.

McKenzie, D., O'Nions, R.K., 1995. The source regions of Ocean Island Basalts. *J. Petrol.* **36** (1), 133–159.

Miller, D.M., Goldstein, S.L., Langmuir, C.H., 1994. Cerium/lead and lead isotope ratios in arc magmas and the enrichment of lead in the continents. *Nature* **368**, 514–520.

Münker, C., Wörner, G., Yogodzinsky, G., Churikova, T., 2004. Behaviour of high-field strength elements in subduction zones: constraints from Kamchatka-Aleutian arc lavas. *Earth Planet. Sci. Lett.* **224**, 275–293.

Ninkovich, D., Robertson, J.H., 1975. Volcanogenic effects on the rates of deposition of sediments in the northwest Pacific Ocean. *Earth Planet. Sci. Lett.* **27**, 127–136.

Nowell, G.M., Kempton, P.D., Noble, S.R., Fitton, J.G., Saunders, A.D., Mahoney, J.J., Taylor, R.N., 1998. High precision Hf isotope measurements of MORB and OIB by thermal ionisation mass spectrometry: insights into the depleted mantle. *Chem. Geol.* **149** (3), 211–233.

Patchett, P.J., 1983. Importance of the Lu–Hf isotopic system in studies of planetary chronology and chemical evolution. *Geochim. Cosmochim. Acta* **47** (1), 81–91.

Patchett, P.J., Tatsumoto, M., 1980. Hafnium variations in oceanic basalts. *Geophys. Res. Lett.* **7**, 1077–1080.

Peacock, S.M., van Keken, P.E., Holloway, S.D., Hacker, B.R., Abers, G.A., Fergason, R.L., 2005. Thermal structure of the Costa Rica—Nicaragua subduction zone. *Phys. Earth Planet. Interiors* **149**, 187–200.

Pearce, J.A., Parkinson, I.J., 1993. Trace element models for mantle melting: application to volcanic arc petrogenesis. In: Prichard, H.M., Alabaster, P.H.M., Harris, N.B.W., Neary, C.R. (Eds.), *Magmatic Processes and Plate Tectonics*, Vol. 76. Geological Science Special Publication, pp. 373–403.

Pearce, J.A., Peate, D.W., 1995. Tectonic implications of the composition of volcanic arc magmas. *Annu. Rev. Earth Planet. Sci.* **23**, 251–285.

Pearce, J.A., Kempton, P.D., Nowell, G.M., Noble, S.R., 1999. Hf–Nd element and isotope perspective on the nature and provenance of mantle and subduction components in western Pacific arc-basin systems. *J. Petrol.* **40** (11), 1579–1611.

Pineau, F., Semet, M.P., Grassineau, N., Okrugin, V.M., Javoy, M., 1999. The genesis of the stable isotope (O,H) record in arc magmas: the Kamchatka's case. *Chem. Geol.* **135**, 93–124.

Pin, C., Joannon, S., Bosq, C., Le Fèvre, B., Gauthier, P.-J., 2003. Precise determination of Rb, Sr, Ba, and Pb in geological materials by isotope dilution and ICP-quadrupole mass spectrometry following selective separation of the analytes. *J. Anal. Atom. Spectrom.* **18**, 135–141.

Plank, T., 2005. Constraints from thorium/lanthanum on sediment recycling at subduction zones and the evolution of the continents. *J. Petrol.* **46** (5), 921–944.

Plank, T., Langmuir, C.H., 1998. The chemical composition of subducting sediment and its consequences for the crust and mantle. *Chem. Geol.* **145**, 325–394.

Portnyagin, M., Hoernle, K., Avdeiko, G., Hauff, F., Werner, R., Bindeman, I., Uspensky, V., Garbe-Schönberg, D., 2005. Transition from arc to oceanic magmatism at the Kamchatka-Aleutian junction. *Geology* **33** (1), 25–28.

Portnyagin, M., Hoernle, K., Plechov, P., Mironov, N., Khubunaya, S., in press. Constraints on mantle melting and composition and nature of slab components in volcanic arcs from volatiles (H_2O, S, Cl, F) and trace elements in melt inclusions from the Kamchatka arc. *Earth Planet. Sci. Lett.*

Ryan, J.G., Morris, J., Tera, F., Leeman, W.P., Tsvetkov, A., 1995. Cross-arc geochemical variations in the Kurile Arc as a function of slab depth. *Science* **270**, 625–627.

Salters, V.J.M., 1996. The generation of mid-ocean ridge basalts from the Hf and Nd isotope perspective. *Earth Planet. Sci. Lett.* **141**, 109–123.

Salters, V.J.M., White, W.M., 1998. Hf isotope constraints on the mantle evolution. *Chem. Geol.* **145** (3), 447–460.

Schmidt A., 2001. Temporal and spatial evolution of the Izu Island arc, Japan, in terms of Sr–Nd–Pb isotope geochemistry. PhD thesis, Geomar Research Center for Marine Geosciences.

Schmidt, M.W., Poli, S., 2004. Generation of mobile components during subduction of oceanic crust. In: Rudnick, R.L. (Ed.), *The Crust*. Elsevier Pergamon, pp. 567–591.

Selyangin, O.B., 1993. New data on Mutnovsky volcano: Structure, evolution and prediction. *Volcanol. Seismol. (in Russian)* **1**, 17–35.

Selyangin, O.B., Ponomareva, V.V., 1999. Gorelovsky Volcanic Center, Southern Kamchatka: Structure and Evolution. *Volcanol. Seismol. (in Russian)* **2**, 3–23.

Stern, R.J., 2002. Subduction zones. *Rev. Geophys.* **40** (4), 1012.

Sun, S.-s., McDonough, W.F., 1989. Chemical and isotopic systematics of oceanic basalts: implications for mantle composition and processes. In: Saunders, A.D., Norry, M.J. (Eds.), *Magmatism in the Ocean Basins*, Vol. 42. Geological Society, pp. 313–345.

Tatsumi, Y., Eggins, S., 1995. *Subduction zone magmatism*. Blackwell.

Taylor, R.N., Nesbitt, R.W., 1998. Isotopic characteristics of subduction fluids in an intra-oceanic setting, Izu-Bonin Arc, Japan. *Earth Planet. Sci. Lett.* **164**, 79–98.

Thorpe, R.S., 1982. *Andesites: Orogenic Andesites and Related Rocks*. John Wiley & Sons, pp. 724.

Tollstrup, D.L., Gill, J.B., 2005. Hafnium systematics of the Mariana arc: evidence for sediment melt and residual phases. *Geology* **33** (9), 737–740.

Turner, S., Hawkesworth, C., Rogers, N., Bartlett, J., Worthington, T., Hergt, J., Pearce, J., Smith, I., 1997. ^{238}U–^{230}Th disequilibria, magma petrogenesis, and flux rates beneath the depleted Tonga-Kermadec island. *Geochim. Cosmochim. Acta* **61** (22), 4855–4884.

Turner, S., McDermott, F., Hawkesworth, C., Kepezhinskas, P., 1998. A U-series study of lavas from Kamtchatka and the Aleutians: constraints on source composition and melting processes. *Contrib. Mineral. Petrol.* **133**, 217–234.

Ulfbeck, D., Baker, J., Waight, T., Krogstad, E., 2003. Rapid sample digestion by fusion and chemical separation of Hf for isotopic analysis by MC-ICPMS. *Talanta* **59**, 365–373.

van Keken, P.E., 2003. The structure and dynamics of the mantle wedge. *Earth Planet. Sci. Lett.* **215**, 323–338.

Vervoort, J.D., Patchett, P.J., Blichert-Toft, J., Albarède, F., 1999. Relationships between Lu–Hf and Sm–Nd isotopic systems in the global sedimentary system. *Earth Planet. Sci. Lett.* **168** (1), 79–99.

Waight, T., Baker, J., Peate, D.W., 2002a. Sr isotope ratio measurements by double-focusing MC-ICPMS: techniques, observations and pitfalls. *Int. J. Mass Spectrom.* **221**, 229–244.

Waight, T., Baker, J., Willigers, B., 2002b. Rb isotope dilution analyses by MC-ICPMS using Zr to correct for mass fractionation: towards improved Rb–Sr geochronology? *Chem. Geol.* **186**, 99–116.

Walker, J.A., Carr, M.J., Patino, L.C., Johnson, C.M., Feigenson, M.D., Ward, R.L., 1995. Abrupt change in magma generation processes across the Central American arc in southeastern Guatemala: flux-dominated melting near the base of the wedge to decompression melting near the top of the wedge. *Contrib. Mineral. Petrol.* **120**, 378–390.

Watson, E.B., Harrison, T.M., 1983. Zircon saturation revisited: temperature and composition effects in a variety of crustal magma types. *Earth Planet. Sci. Lett.* **64**, 295–304.

Workman, R.K., Hart, S.R., 2005. Major and trace element composition of the depleted MORB mantle (DMM). *Earth Planet. Sci. Lett.* **231**, 53–72.

Yogodzinski, G.M., Lees, J.M., Churikova, T.G., Dorendorf, F., Wöerner, G., Volynets, O.N., 2001. Geochemical evidence for the melting of subducting oceanic lithosphere at plate edges. *Nature* **409**, 500–504.